NASA CONTRACTOR REPORT
NASA CR - 134641

CYCLIC FATIGUE ANALYSIS OF ROCKET THRUST CHAMBERS: VOLUME I — OFHC COPPER CHAMBER LOW CYCLE FATIGUE

by

Roy W. Miller

Atkins & Merrill Inc.

Ashland, Mass.

June 1974

Prepared for

NATIONAL AERONAUTICS AND SPACE ADMINISTRATION
Lewis Research Center
Cleveland, Ohio

Contract NAS 3-17807
H.G. Price, Project Manager

CONTENTS

PREFACE

A previous report, Reference 1, prepared under this contract, described a computer program, designated RETSCP, for the analysis of rocket engine thrust chambers with cyclic plasticity. That report included a complete description of the program logic, together with a users manual. It is the purpose of this report to illustrate the detailed application of the RETSCP program. Volume I describes the analysis of a regeneratively cooled OFHC copper combustion chamber. Operating conditions are such that plastic strains dominate and fatigue life is in the low cycle regime. Volume II describes the analysis of an attitude control thrust chamber. Operating conditions for that engine are such that the material behavior is elastic, or on the threshold of the elasto-plastic regime; thus, the fatigue life is in the high cycle regime.

SUMMARY

A three-dimensional finite element elasto-plastic strain analysis was performed for the throat section of a regeneratively cooled rocket combustion chamber. The analysis employed the RETSCP finite element computer program (NASA CR-134640). The analysis included thermal and pressure loads, and the effects of temperature dependent material properties, to determine the strain range corresponding to the chamber operating cycle. The analysis was performed for chamber configuration and operating conditions corresponding to a hydrogen-oxygen combustion chamber which was fatigue tested to failure at the NASA Lewis Research Center. The computed strain range at typical chamber operating conditions was used in conjunction with OFHC copper isothermal fatigue test data to predict chamber low-cycle fatigue life.

INTRODUCTION

A new generation of high performance liquid rocket engines is being considered for main propulsion in Space Transportation Systems. The high performance goal which has been established for these engines demands high chamber pressures with resulting high heat flux levels in the combustion chamber. For Space Transportation System applications, engine reusability is a prime objective. Thus, the stress analyst must be able to define the life potential of a given design under conditions of thermal and pressure cycling.

Combustion chambers can be designed to operate at suitable temperature levels by employing regenerative cooling. The combination of high heat flux and high pressure necessitates the use of materials with high thermal conductivity. Such materials permit practical values of wall thickness without creating excessive hot gas side wall temperatures. Typical construction consists of a copper based alloy combustion liner, containing milled coolant passages, combined with a nickel alloy structural jacket. The thermal analysis of combustion chambers such as this follows established methodology. Empirical data is available for estimating combustion gas and coolant heat transfer. The temperature distribution within the structure is computed using one of many available finite difference computer codes for transient or steady state heat conduction in two or three dimensions.

The state of stress in regeneratively cooled rocket chambers varies in three dimensions. The situation is further complicated by the strong dependence of material properties on temperature. It is the range of strain,

through which a given chamber is cycled, that determines fatigue life. A numerical method of structural analysis must be employed for such complex configurations.

The objective of Volume I is twofold. First, there is the application of a three dimensional finite element computer program to determine the thermal strain behavior of a specific regeneratively cooled copper combustion chamber. An indepth study of this type, not only provides strain range data for fatigue life analysis; but also lends insight into the structural response of the chamber under complex loading conditions. The copper chamber configuration and operating conditions correspond to a chamber which was fatigue tested to failure at the NASA Lewis Research Center.

The second objective is to illustrate in detail the use of the RETSCP finite element computer program for chamber configurations where plastic strains dominate; that is, low cycle fatigue. Thus, considerable attention is given to the finite element model, material properties, and execution of the program.

The combustion chamber configuration, operating conditions, and test results are described in sufficient detail to conduct the strain analysis and compare results. The strain analysis is then presented in such a manner that the work could be extended to other configurations and operating conditions. The fatigue life analysis section describes the

predictive method used for the copper chamber; and, also indicates methods which could be employed for other studies. The Concluding Remarks include discussion of future applications for the RETSCP computer program, including refinements for fatigue life prediction, and phenominalogical studies of the thermal strain behavior.

COMBUSTION CHAMBER CONFIGURATION

The fatigue life analysis was conducted for the throat section of a specific regeneratively cooled rocket thrust chamber which was fatigue tested to failure at the NASA Lewis Research Center. Since the experimental results are unpublished, those facets of the geometry, operating conditions, and test data which pertain to the life analysis are given below.

Chamber Geometry

The overall combustion chamber geometry and construction data are shown in Figure 1. The basic component of the chamber for high heat flux and high pressure is the OFHC copper liner. This liner contains sixty milled axial coolant flow passages. The high thermal conductivity of the copper produces two beneficial effects. First, from a manufacturing standpoint, the material permits practical values of wall thickness. The allowable hot wall operating temperature, together with the imposed heat flux value, determine the wall thickness. Thus, for materials with low thermal conductivity, such as nickel alloys, extremely thin walls are required. The second effect, due to high thermal conductivity, is that the ribs which divide the cooling passages are very effective as cooling fins.

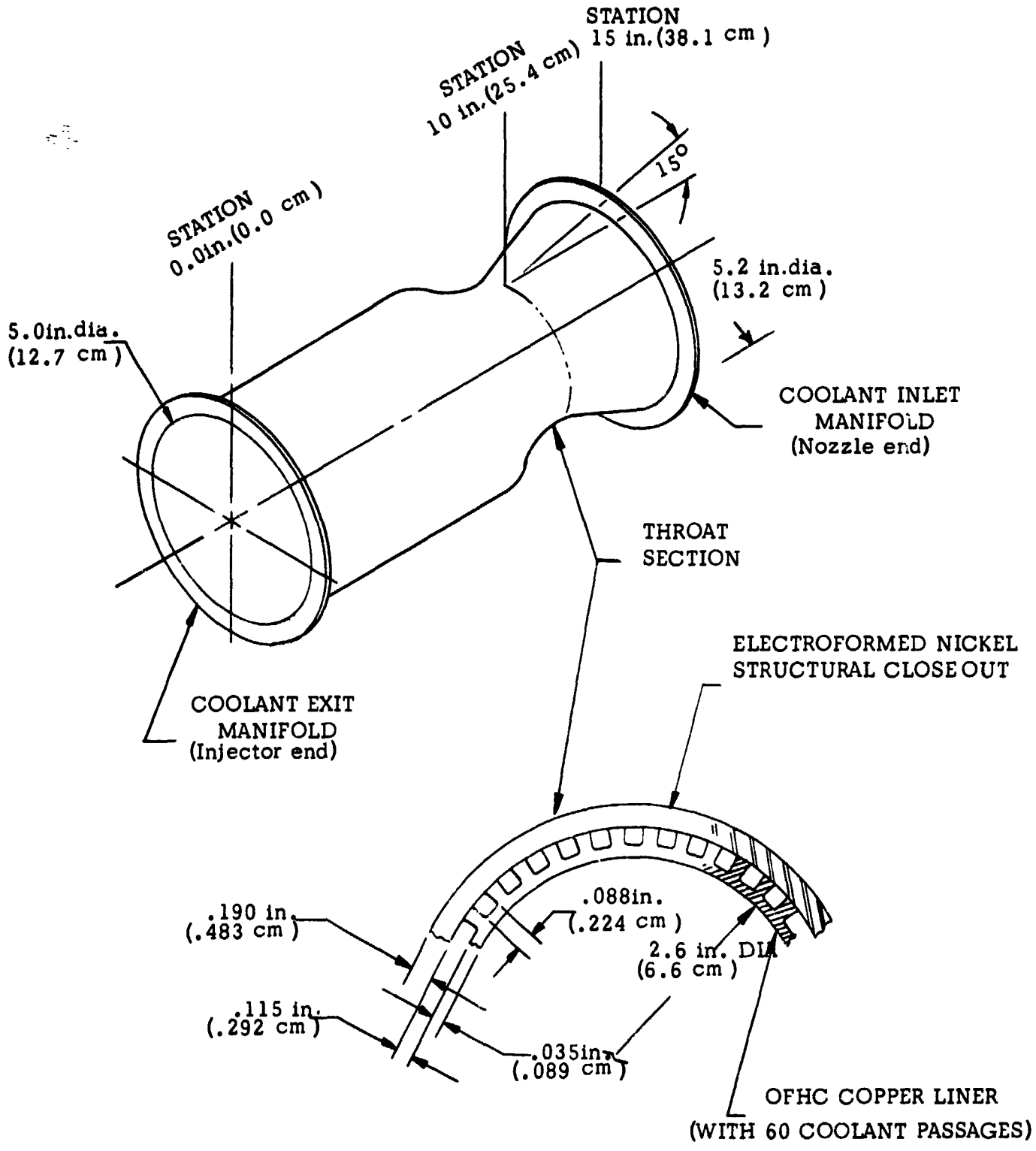

Figure 1. Combustion chamber geometry.

Chamber structural integrity is maintained by the electroformed nickel closeout jacket. The nickel has low thermal conductivity (as compared with copper); and, therefore, low temperatures are encountered throughout the operating cycle. Thus, the nickel jacket restrains the chamber pressure hoop and thrust loads during engine operation, Note, that the nickel structure contains integral coolant manifolds; and, that the coolant flow direction is from chamber nozzle toward engine injector.

The chamber is instrumented to measure chamber and coolant pressures as well as coolant inlet and outlet temperature. At the throat section, the nickel jacket and copper liner temperatures are measured at four circumferential stations. Nickel jacket thermocouples are attached to the outer wall surface. Copper liner thermocouples are located nominally at 0.050 in. (0.127 cm) from the hot gas side surface, circumferentially centered within the liner ribs. One rib temperature thermocouple was inoperable due to damage during chamber fabrication.

Operating Conditions

The fatigue test thrust chamber is a regeneratively cooled hydrogen-oxygen chamber which is cooled by cold hydrogen near $50^{\circ}R$ ($28^{\circ}K$) inlet temperature and 1066 psia (7.35×10^{6} N/m^{2}) inlet pressure. Coolant flow preceeds chamber firing and by-passes the chamber; thus, producing precool to a uniform temperature near $50^{\circ}R$ ($28^{\circ}K$).

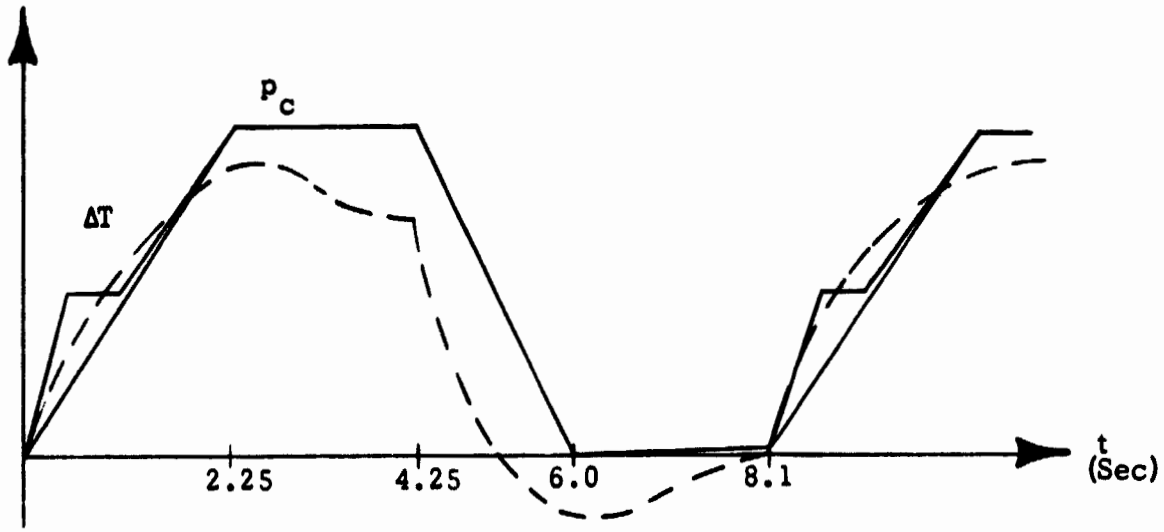

Figure 2. Thrust chamber operating cycle.

The thrust chamber pressure pulse is indicated by the solid line curve in Figure 2. During the chamber start transient, the chamber pressure is increased to 610 psia (4.21×10^6 N/ m^2) in a 2.25 second interval. The step transient start is required by facility limits. Measured thrust force during the 2.0 second operating phase was 4686 lbs. (20840 N). Thrust chamber shutdown occurs over a 1.75 second interval. The hydrogen coolant bypass flow is maintained for the 2.1 second period between pulses. The test chamber was subjected to pulse trains consisting of one to eleven pulses of the type described.

Combustion gas conditions at the throat station are 347 psia (2.39×10^6 N/m^2) static pressure and 6143°R (3413°K) adiabatic wall temperature. Coolant temperature and pressure at the throat during steady state firing are 132°R (73°K) and 1045 psia (7.21×10^6 N/ m^2) respectively.

Test Results

The measured temperature response at the chamber throat is depicted by the dashed line curve (Δ T) in Figure 2. The value Δ T represents the difference between the measured copper liner temperature and the nickel jacket outer wall temperature. During the engine start transient, the copper liner heats at a greater rate than the low conductivity nickel jacket. After the copper has reached steady state temperature, the nickel approaches steady state conditions; thus, generating the thermal overshoot in Figure 2. A similar cooling overshoot occurs during thrust chamber shutdown.

The thrust chamber was tested at the operating conditions previously described for pulse trains of 1,1,1,1,5,4,3,11,1,2,3,5,3,2 pulses each for a total of forty-three cycles. Visual inspection after forty-third pulse revealed a thru-crack from the coolant passage to the combustion chamber interior at the chamber throat. The thru-crack probably occured on the thirty-ninth cycle when a change in the test cell noise pattern was perceived.

It should be noted that geometric changes were observed along the combustion chamber length as the test program progressed, coolant channel bulging and surface roughening of the hot gas side copper surface occurred. These effects were apparent after only a few cycles of testing. Associated with these changes, the thermal characteristics of the engine were altered, and the measured copper temperature levels showed a gradual increase with each successive firing.

STRAIN ANALYSIS

It is well known that fatigue life depends on the cyclic strain range magnitude. One could compute the strain range for each loading cycle using the RETSCP program, Reference 1, and determine the amount of fatigue damage by applying the linear cummulative damage law, Reference 2. In the interest of computional practicality, the strain analysis is based on a set of typical or average material properties.

Finite Element Model

The RETSCP strain analysis employed the thirty-four element model of the copper chamber throat section shown in Figure 3. The cross section shown is one of 120 similar symmetry sections. Each element has the same thickness of 0.010 in. (0.025 cm) in the z - direction. Of course, the throat station was chosen for analysis since it is the location of the extreme thermal condition.

The number of elements was selected to adequately represent the structure, More elements were used in locations where large changes in strain and temperature are expected; for example, near the hot gas side surface. It was noted in Reference 1, that the RETSCP program is based on an isoparametric element; and thus, few elements are required to model the structure.

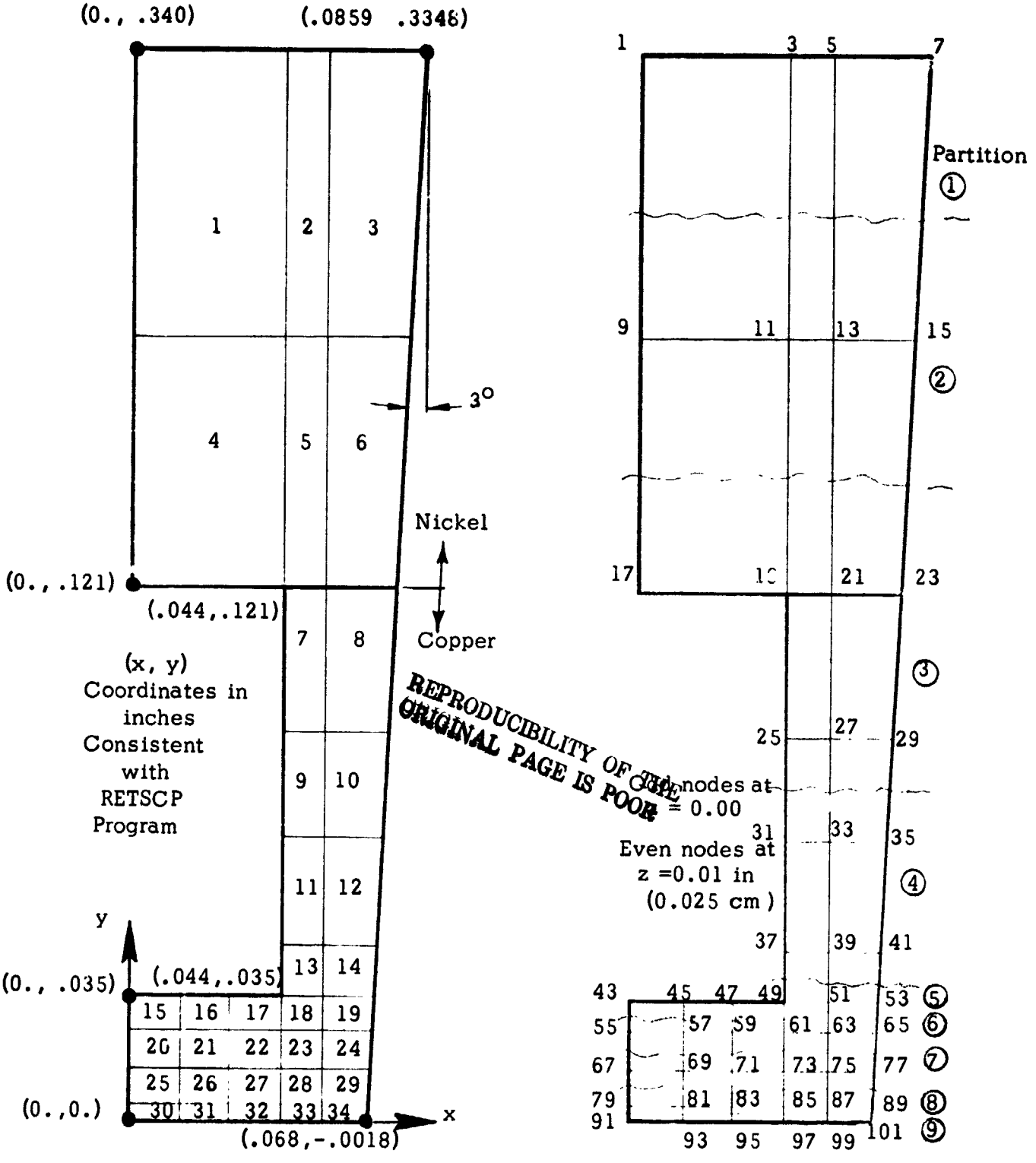

(a) Geometry and Element Numbers

(b) Node Numbers and Partition Numbers

Figure 3. Finite element model.

Boundary conditions in the RETSCP program are in the form of prescribed nodal point forces or nodal point displacements. The symmetry of the 34 - element model was previously noted. The corresponding boundary condition is zero displacement of boundary points normal to the symmetry plane, and free movement of nodal points in the radial direction. This condition is indicated by the roller notation in Figure 4. The symmetry condition along the 3^{o} surface is accommodated by a coordinate transformation within the RETSCP program.

The surfaces exposed to the coolant and combustion gasses experience prescribed force in the direction normal to the surface. The pressure is replaced by force components at each nodal point as indicated in Figure 4. Each point carries load from adjacent pressure surfaces. Of course, the force components on the combustion surface are zero for engine-off conditions.

The boundary conditions in the z - direction require special consideration. A very thin section is taken at the throat, so that the rocket engine contour curvature can be neglected. That is, constant thickness elements are used. Under load, the section remains plane; and also, the total load on the section is equal to the engine thrust load. This corresponds to the generalized plane strain condition.

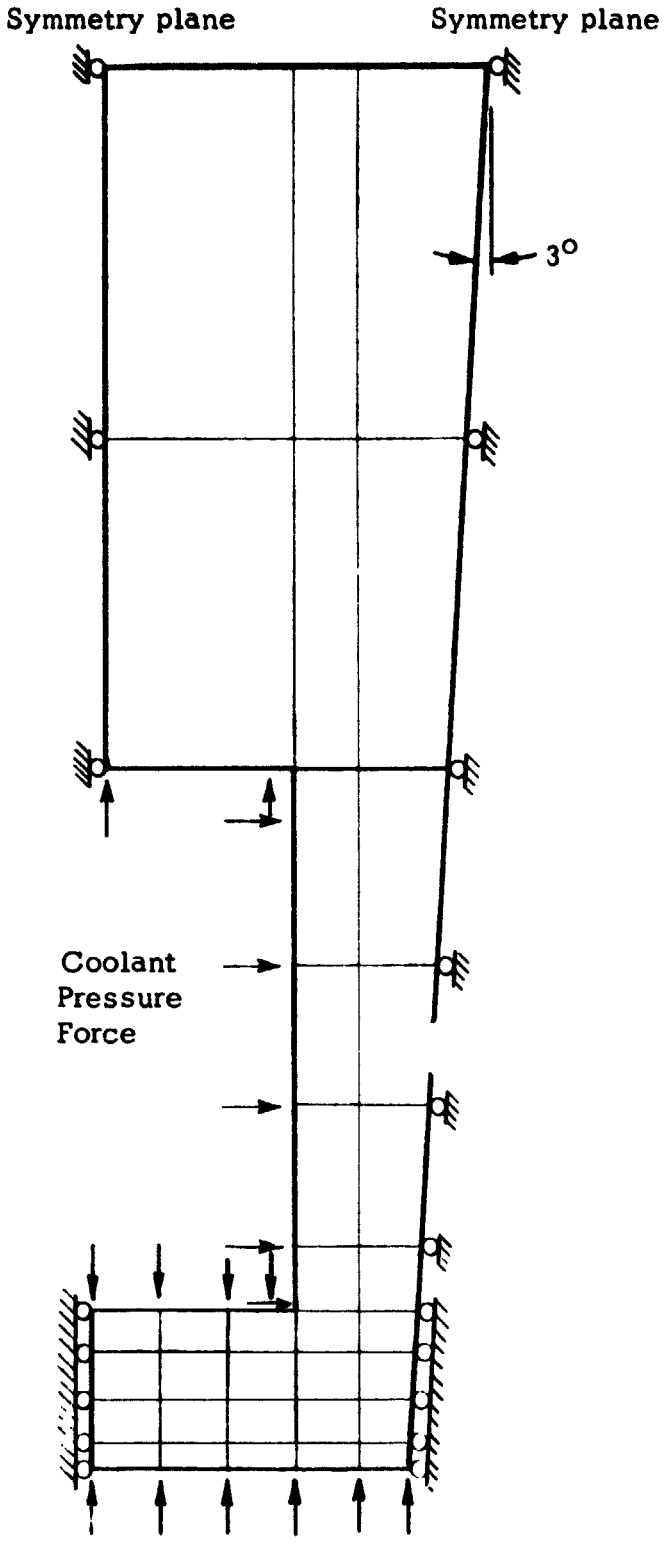

Figure 4. Force and displacement (symmetry) boundary conditions.

Recall that in the RETSCP program, either forces or displacements are prescribed at the nodal points. In this case, we prescribe zero displacement of all points on one face, and a single displacement value for all points on the opposite face. Since the nodal point forces are output by the RETSCP program, we make a posteriori check that the sum of the forces in the z - direction equals the thrust force. If not, the z - displacement is adjusted and the process repeated.

The initial displacement estimate is based on the generalized plane strain equation applied to the nickel closeout structure; namely, Reference 4, (Symbols are defined in Appendix A)

$$\epsilon_z = \frac{1}{E}\left[\sigma_z - \nu(\sigma_x + \sigma_y)\right] \qquad (1)$$

Stresses in the y- direction are neglected. The x - stress in the nickel is approximated by the pressure hoop stress. That value is adjusted due to the thermal expansion force exerted by the copper liner in the hoop direction. The copper is at yield stress conditions. Similarly, the z - stress is approximated by the axial thrust stress which is corrected due to the force exerted by the copper in the axial direction at yield stress conditions. The computed strain is then converted to displacement, and adjusted by the average thermal growth of the nickel to give the initial prescribed displacement estimate.

Thus, the terms in equation (1) are:

$$\sigma_x \simeq \frac{\frac{1}{2}\left[\text{internal pressure}\right]\left[\text{throat diameter}\right] + \left[\text{average copper yield stress}\right]\left[\text{copper radial thickness at coolant passage}\right]}{\left[\text{nickel radial thickness}\right]}$$

$$\sigma_y \simeq 0$$

$$\sigma_z \simeq \frac{\left[\text{thrust}\right] + \left[\text{average copper yield stress}\right]\left[\text{copper cross sectional area}\right]}{\left[\text{nickel cross sectional area}\right]}$$

In principle, the above procedure will lead to a consistent set of results with the proper axial force solution. In the case of the copper chamber, the copper strain behavior is so dominated by the thermal growth, that the small axial displacement value has little effect. Thus, correction of the initial guess value is not warranted; and, although the stress field in the nickel may be somewhat erronious, the strain range of the copper liner is not effected.

Temperature Distribution

A complete thermal analysis was performed for the regeneratively cooled copper combustion chamber. The calculation of heat transfer coefficients, overall heat balance, and coolant properties was performed by NASA and is furnished data.

Transient heat conduction temperature distributions were computed for an 89 node model of the configuration shown in Figure 3, by using a

finite difference computer program. Based on the computer output, interpolation was used to obtain the average temperature for each of the 34 finite elements, Figure 3.

The predicted temperature values, corresponding to the measurement locations, showed excellent agreement with the values measured during the first few cycles of testing. As previously noted, the measured temperature values showed a gradual increase as testing progressed. Thus, the temperature distributions were recomputed with input boundary conditions such that results would agree with temperature values from the twentieth test cycle. The twentieth cycle is approximately one half of the chamber life; and, is thus assumed to represent average or typical conditions. Input conditions were selected in the program such that computed results agreed with the thermocouples in the copper liner. Measured values on the nickel were somewhat lower than the recomputed values which indicated that convection to the surroundings and axial conduction heat transfer were significant. The nickel elements were further adjusted to account for this deviation.

The NASA furnished sets of temperature data for the finite element model are listed in Table I, for the four critical points of the operating cycle indicated in Figure 2; that is; (a) precool-intercool, (b) start transient peak overshoot, (c) steady state chamber firing, and (d) cooldown transient peak overshoot. Sample results, taken from the four sets of 34 temperature difference values are shown in Figure 5. Note that the maximum temperature value is $1493^{\circ}R$ (829° K) which corresponds to the temperature difference of $993^{\circ}R$ (552° K), which occurs during the steady state chamber firing. Temperature differences in Table I and Figure 5 are in units ($^{\circ}R$) suitable for the RETSCP program.

TABLE I

NASA FURNISHED TEMPERATURE DIFFERENCE* ($\Delta T = T - T_{ref}$) FOR TWENTIETH TEST CYCLE ($T_{ref} = 500^{\circ}R$).

Element	Δ Ta (t=0 or 8.1 sec)	Δ Tb (t= 2.4 sec)	Δ Tc (t= 4.2 sec)	Δ Td (t= 6.0 sec)
1	-450.	-153	+92	-135
2	-450.	-153	+95	-135
3	-450.	-153	+95	-135
4	-450.	-30	+127	-219
5	-450.	+18	+170	-224
6	-450.	+37	+189	-224
7	-450.	+235	+330	-264
8	-450.	+249	+344	-262
9	-450.	+316	+401	-278
10	-450.	+327	+413	-275
11	-450.	+483	+557	-290
12	-450.	+493	+568	-288
13	-450.	+601	+671	-295
14	-450.	+606	+677	-293
15	-450.	+830	+893	-303
16	-450.	+814	+877	-302
17	-450.	+776	+841	-300
18	-450.	+727	+794	-297
19	-450.	+708	+776	-295
20	-450.	+847	+905	-302
21	-450.	+839	+903	-302
22	-450.	+799	+864	-300
23	-450.	+753	+820	-297
24	-450.	+743	+812	-296
25	-450.	+885	+947	-302
26	-450.	+878	+941	-302
27	-450.	+846	+911	-300
28	-450.	+817	+882	-298
29	-450.	+809	+875	-298
30	-450.	+931	+993	-304
31	-450.	+912	+975	-302
32	-450.	+896	+959	-301
33	-450.	+876	+941	-300
34	-450.	+864	+930	-300

*Note: Values are in $^{\circ}R$ ($1.8 \times ^{\circ}K$) which is suitable unit for RETSCP.

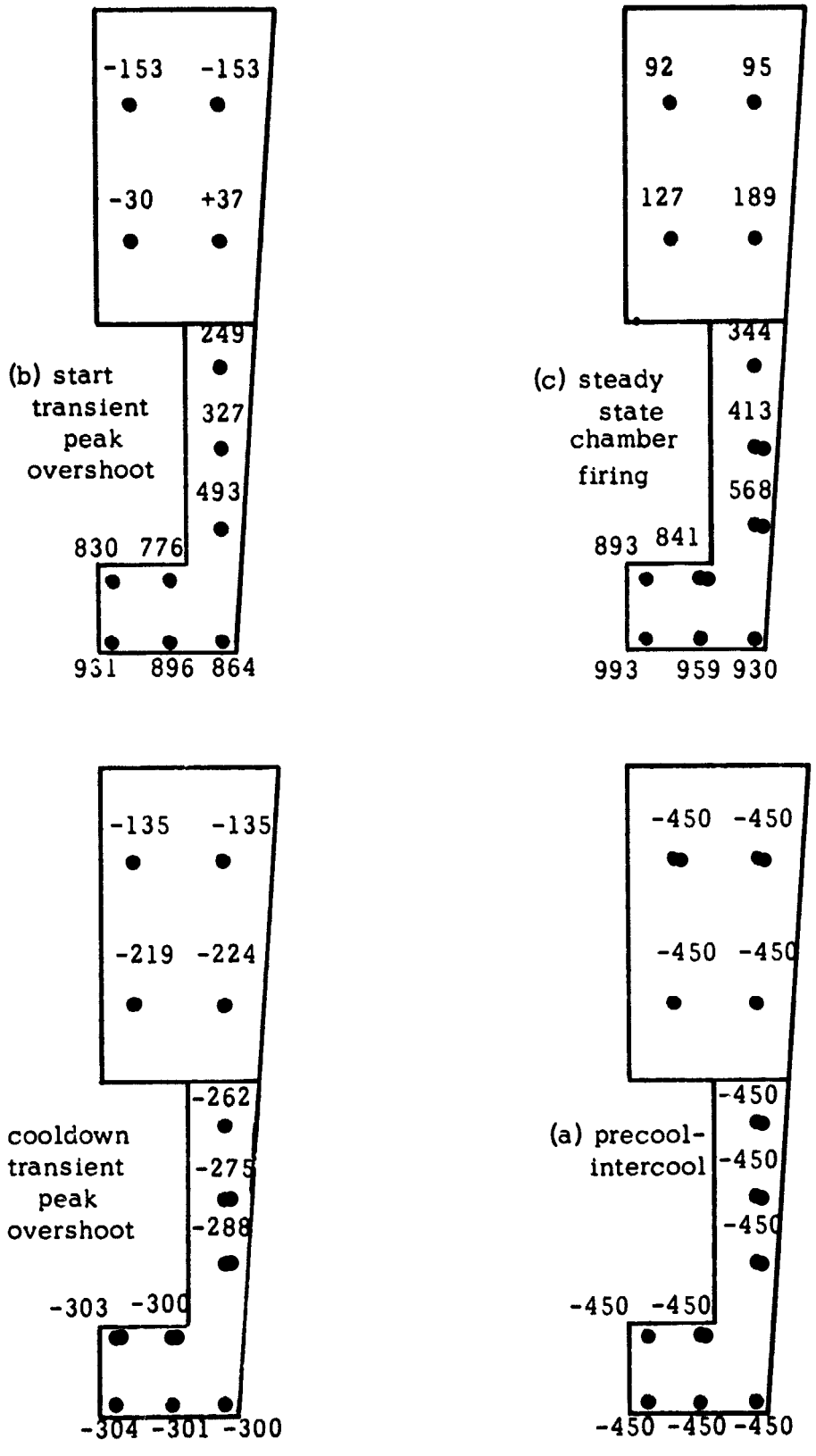

Figure 5. Computed temperature difference ($\Delta T = T - T_{ref}$) for twentieth test cycle ($T_{ref} = 500^{\circ}R$). Values are in $^{\circ}R$ ($1.8 \times {}^{\circ}K$) which is suitable unit for RETSCP.

Material Properties

Materials properties are input as functions of temperature in the RETSCP program. Also, RETSCP plasticity analysis is based on bi-linear representation of the uniaxial test stress strain curve. It is well known that materials such as OFHC copper, work harden, or work soften, or harden then soften upon plastic strain cycling, Reference 5. Experimentally determined stress-strain curves are seldom available as functions of temperature and the number of strain cycles. Thus, it is necessary to construct stress-strain curves based on theory together with the best available experimental data.

It turns out that for plastic behavior, the true stress-true strain curve appears as a nearly straight line when plotted on logarithmic coordinates, Reference 6. Room temperature data for annealed OFHC copper, Reference 7, is presented by the open circles in Figure 6. Other curves were constructed and are shown in Figure 6, based on the 0.2 % offset yield stress, and the ultimate tensile stress at 40% strain which is assumed to correspond to the start of necking for annealed OFHC copper as reported in Reference 8. These data all apply for virgin material.

The cyclic stress-strain curve, Reference 9, has great value for strain cycle calculations. Such curves are constructed with the aid of fatigue test data. The test strain range, together with the measured stress range which occurred at one-half the number of cycles to failure, defines a point on the cyclic stress-strain curve.

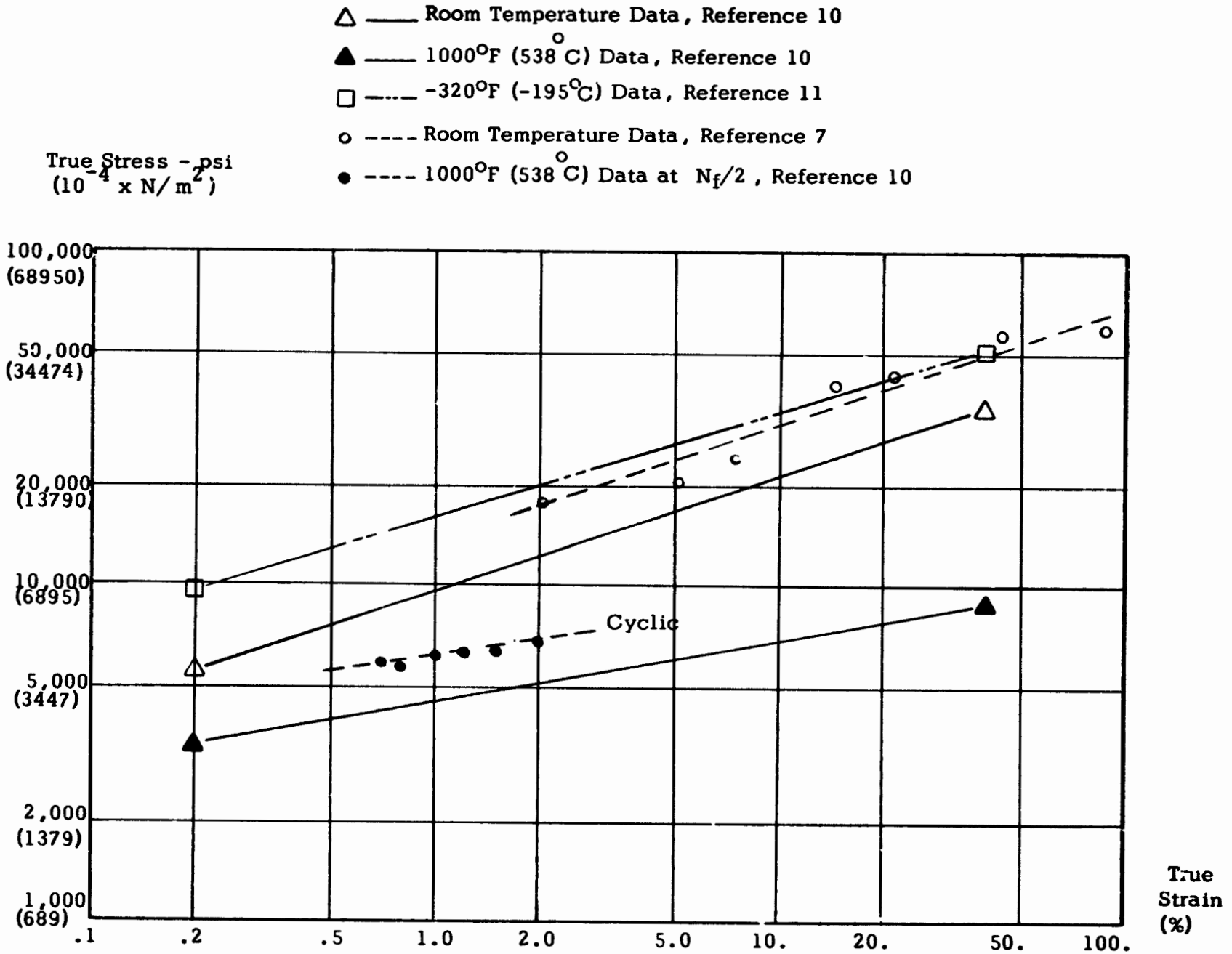

Figure 6. True stress - true strain curves for OFHC copper

The cyclic stress-strain curve for annealed OFHC copper, shown in Figure 6, is based on copper fatigue test data, Reference 10, at 1000°F (538°C) (closed circles). The effect of cyclic work hardening is quite clear (about 30%). Since strain hardening of copper occurs in the first few cycles, work hardening is accounted for by using the cyclic stress strain curves.

The stress-strain data are replotted in Figure 7 for strain values up to 3%. The plastic portion of the curves were constructed directly from Figure 6. The pre-yield portion of the curves, in Figure 7, are faired curves to smoothly connect the linear elastic curve, based on modulus, to the plasticity data. The cyclic data in Figure 7 shows 30% hardening (stress increase over virgin material) at 3% strain.

Cyclic stress strain curves at other temperatures were constructed by increasing the stress 30% at 3% strain and redrawing the curve to the same shape. Results are shown by the dash line curves in Figure 8. The bi-linear representations, which were used for the rocket chamber strain calculation, are shown by the solid lines in Figure 8. Stress-strain data at intermediate temperature values is computed within the program by linear interpolation between the values shown in Figure 8.

Note, that for small elasto-plastic strain values (less than 0.5%), the bi-linear approximations in Figure 8 do not approximate the actual curve very well. Thus, a set of bi-linear curves for strains up to 0.5% were

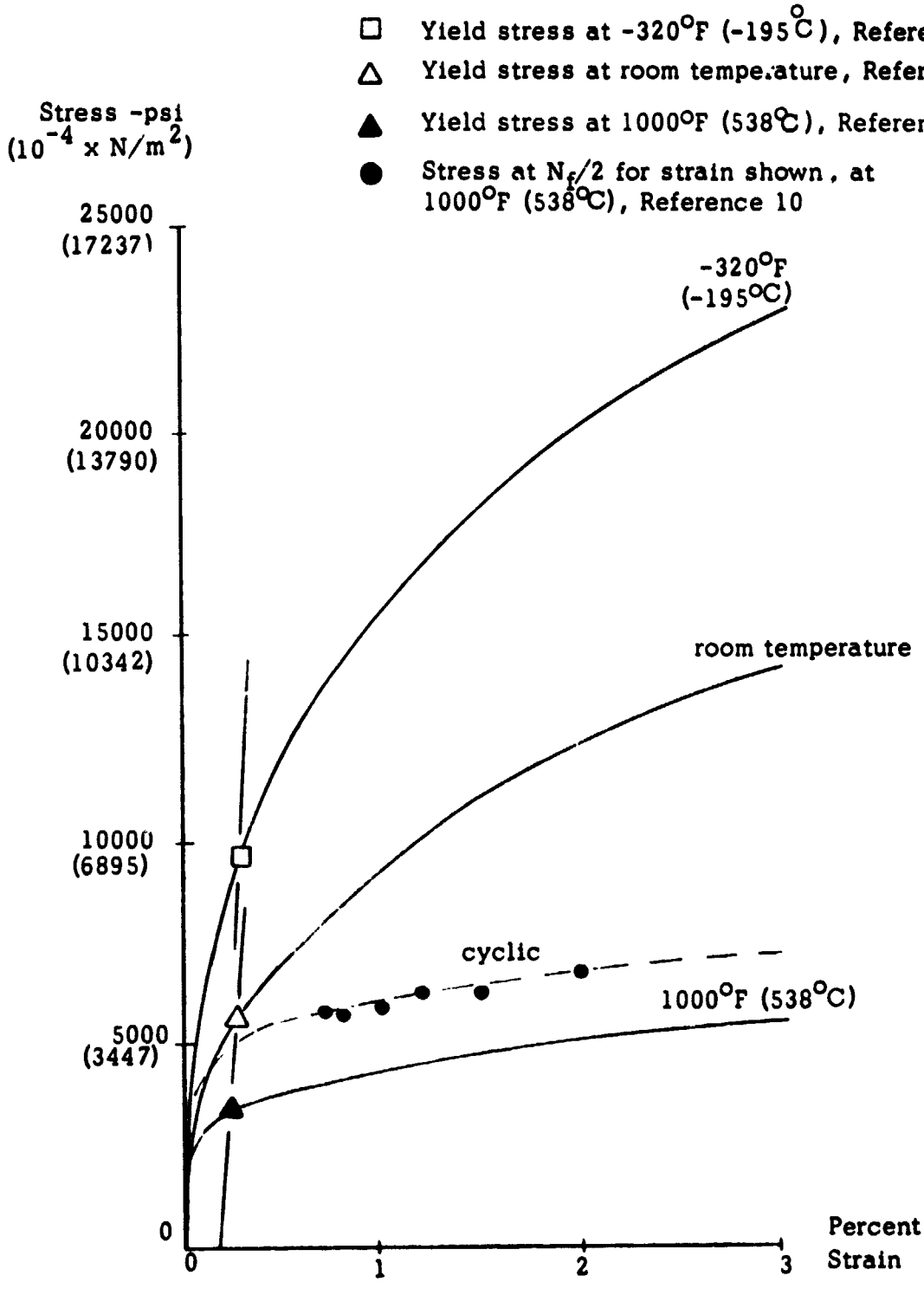

Figure 7. Stress-strain curves for OFHC copper

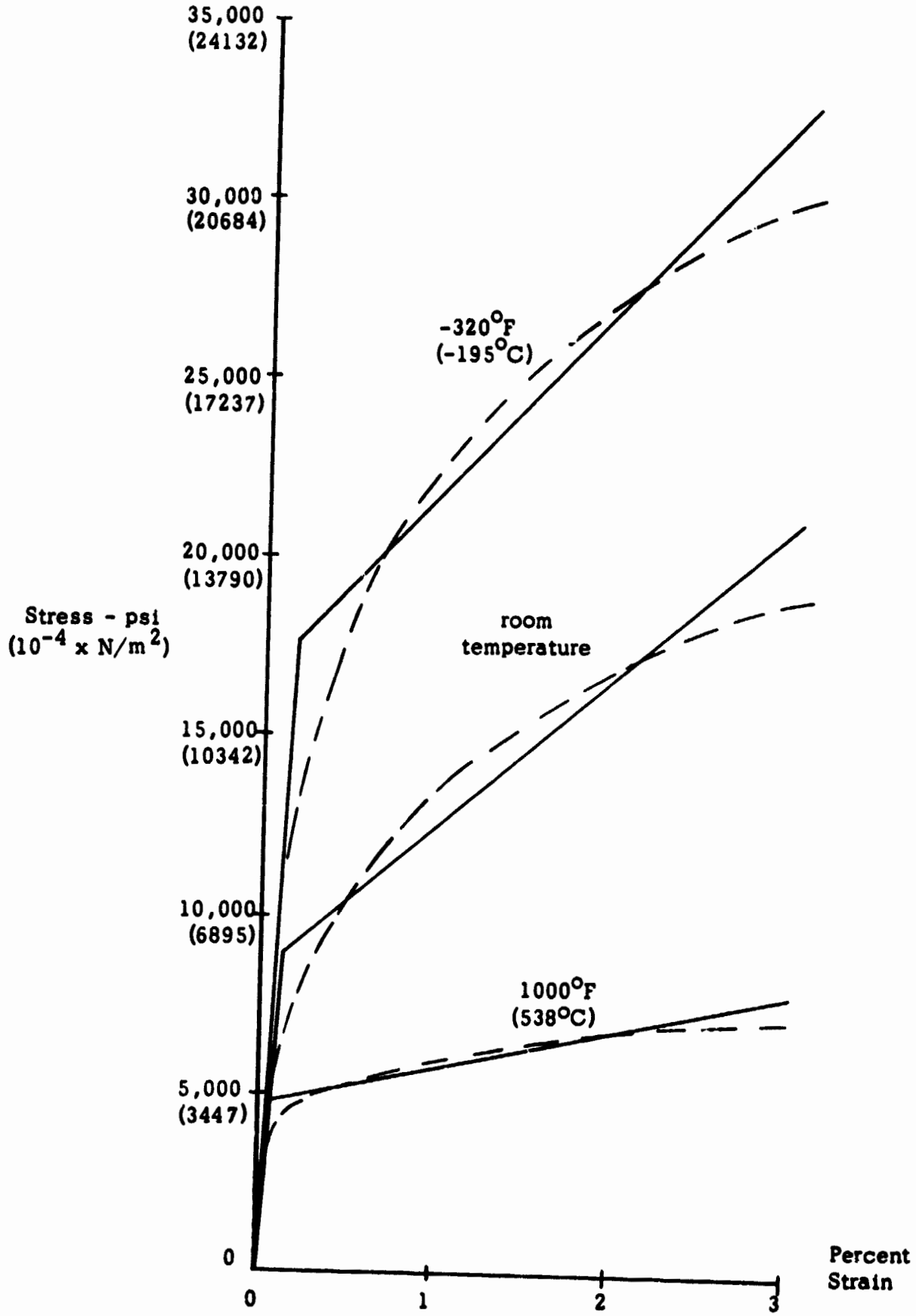

Figure 8. Bi-linear cyclic stress-strain curves for OFHC copper up to 3 percent strain.

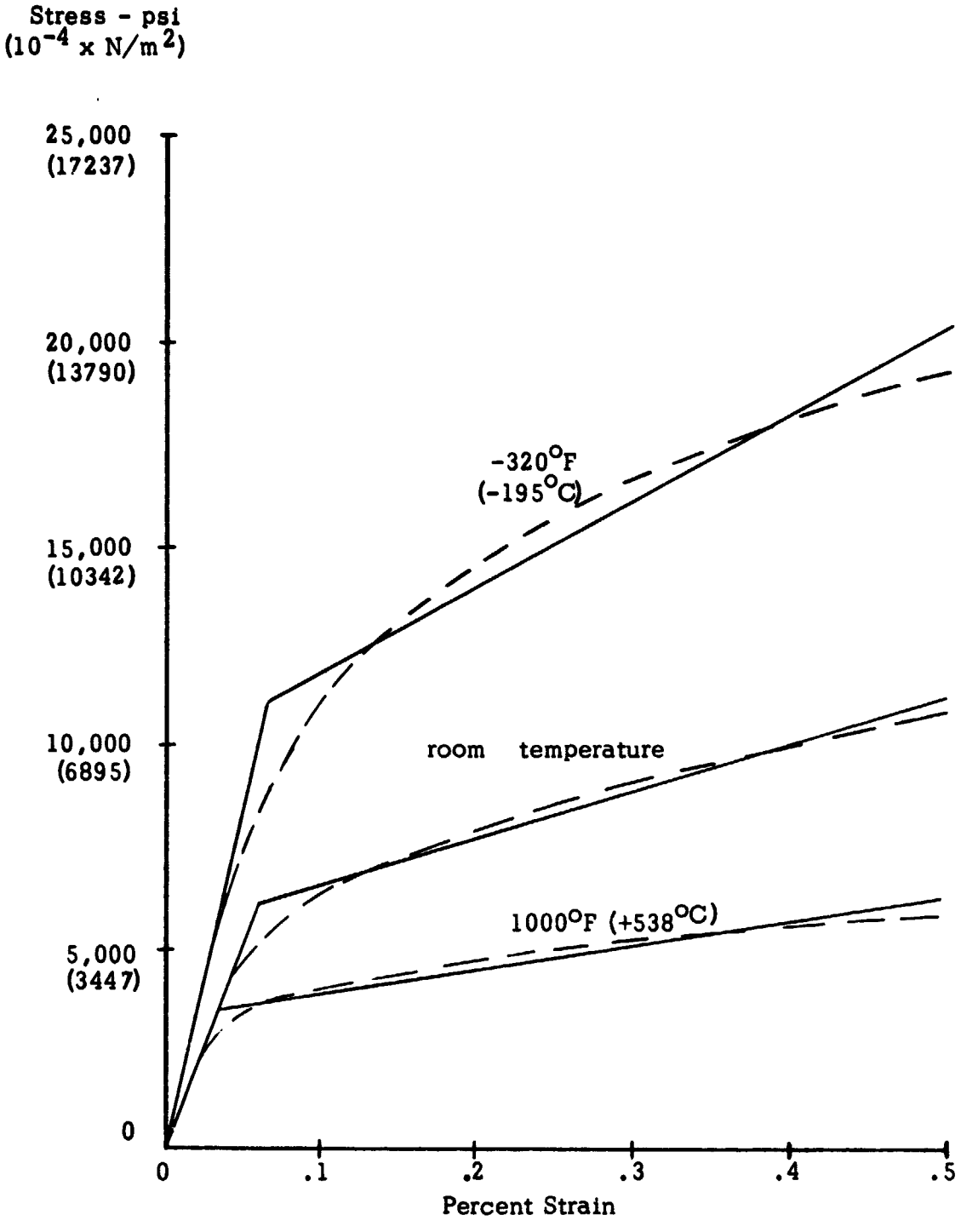

Figure 9. Bi-linear cyclic stress-strain curve for OFHC copper up to 0.5 percent strain.

constructed, and are presented in Figure 9. Specifically, these curves were used in the analysis for element number 7,8,9 and 10. The applicability of this strain level for those elements will be apparent later.

A summary of all data used in the RETSCP program for the OFHC copper combustion chamber is given in Table II.

Structural Analysis

First, let us qualitatively examine the structural behavior of the combustion chamber as it is subjected to operating conditions and thermal loading such as depicted in Figure 2 and 5.

The chamber is initially subjected to a $50^{\circ}R$ ($28^{\circ}K$) precool temperature in combination with the coolant pressure load. Since the copper has a larger coefficient of thermal expansion (contraction) than the nickel, precool tensile stresses result in the copper and precool compressive stresses are induced in the nickel jacket. The high strength nickel jacket is sufficiently massive to remain elastic; however, the copper stress level may be high enough that yielding of the copper occurs.

Upon heating to the start transient peak overshoot level, the situation is reversed. The large amount of thermal growth of the copper liner generates plastic compressive deformation. The nickel structure behaves elastically in tension to resist the chamber pressure hoop loading.

TABLE II

SUMMARY OF MATERIALS PROPERTY DATA

Property	English Units (RETSCP)	Metric Units
Thermal Expansion Coefficient:		
Nickel	7.2×10^{-6} in/in-°F	13.0×10^{-6} m/m-°C
Copper	9.8×10^{-6} in/in-°F	17.6×10^{-6} m/m-°C
Modulus of Elasticity:		
Nickel	$30.0 \times 10^{+6}$ psi	$20.7 \times 10^{+10}$ N/m^2
Copper-cold	$16.6 \times 10^{+6}$ psi	$11.4 \times 10^{+10}$ N/m^2
Copper-hot	$10.0 \times 10^{+6}$ psi	$6.9 \times 10^{+10}$ N/m^2
Poisson's Ratio:		
Nickel	.31	.31
Copper	.33	.33
Yield Stress: ($\sigma_y = \sigma_0 - \lambda_1 T$)		
Nickel	55,000 psi	$379. \times 10^{+6}$ N/m^2
Nickel	0.	0.
Copper Large Strain (σ_0) -hot	9,200 psi	$63.4 \times 10^{+6}$ N/m^2
Copper Large Strain (λ_1) -hot	4.63 psi/°F	$5.75 \times 10^{+4}$ N/m^2-°C
Copper Small Strain (σ_0) -hot	6,000 psi	$4.14 \times 10^{+4}$ N/m^2
Copper Small Strain (λ_1) -hot	2.63 psi/°F	$3.26 \times 10^{+4}$ N/m^2-°C
Copper Large Strain (σ_0) -cold	17,700 psi	$11.7 \times 10^{+7}$ N/m^2
Copper Large Strain (λ_1) -cold	0.	0.
Copper Small Strain (σ_0) -cold	11,000 psi	$75.8 \times 10^{+6}$ N/m^2
Copper Small Strain (λ_1) -cold	0.	0.
Plastic Modulus Ratio: ($m = m_o \times 10^{-3} - \lambda_2 T \times 10^{-6}$)		
Copper Large Strain (m_o) -hot	41.7	41.7
Copper Large Strain (λ_2) -hot	33.1 $^1/_{°F}$	59.6 $^1/_{°C}$
Copper Small Strain (m_o) -hot	117.7 $^1/_{°F}$	211.9 $^1/_{°C}$
Copper Small Strain (λ_2) -hot	6.32	6.32
Copper Large Strain (m_o) -cold	31.7	31.7
Copper Large Strain (λ_2) -cold	0.	0.
Copper Small Strain (m_o) -cold	132.	132.
Copper Small Strain (λ_2) -cold	0.	0.
Nickel (m_o)	1.0	1.0
Nickel (λ_2)	0.	0.

The stress-strain condition at steady state chamber firing may introduce a variety of effects. Just as the nickel-to-copper temperature difference is relaxed; so is the thermal strain level relaxed. The important point is that this relaxation takes place along the elastic line. This point will be illustrated later. The strain relaxation may terminate either with tensile or compressive elastic stresses in the copper; or, relaxation may be sufficiently great to generate tensile plastic deformation.

The cooldown transient peak overshoot corresponds to the maximum strain state under cold conditions. As the chamber returns to uniform intercool conditions, $50^{\circ}R$ ($28^{\circ}K$) with coolant pressure loading, relaxation type behavior will again be exhibited.

The second test cycle will produce similar qualitative behavior with two major differences. First, the residual strain values, for all segments of the cycle, will differ from the first loading cycle. Second, the material will have work hardened as a result of deforming plastically. A few loading cycles will "shake-down" the effect of the residual strain starting point. Also, strain hardening of the copper will diminish after a few cycles, Reference 12 and 13. For the present calculation, work hardening is not accounted for on a cycle by cycle basis; rather, hardening is included through the use of cyclic stress strain data. Thus, a repeatable hysteresis strain cycle will eventually be established. It is noteworthy, that, the maximum strain range for any cycle will be determined by the peak to peak variations in nickel-to-copper temperature difference.

RETSCP Program Execution

The detailed copper chamber strain cycle was computed using the 34 element model shown in Figure 3. In the absence of cycle-by-cycle strain hardening data, the cyclic stress-strain curves presented in Figures 8 and 9, and discussed previously, were employed. Other input material properties are listed in Table II. Pressure loads and boundary conditions correspond to Figure 4. Thermal loads were based on the twentieth cycle temperature differences given in Table I and Figure 5. Thus, the calculated strain cycle corresponds to an average or typical test cycle.

Each computer run consists of strain analysis based on one set of operating conditions together with one set of prestrain data. The calculation starts by introducing the precool condition (a) from Table I together with cold material properties data and zero chamber pressure. The RETSCP program output consists of a stress-strain listing plus punch card residual strain data for each element. The punch cards are entered with condition (b) temperature in Table I; and, using the hot material properties data and maximum chamber pressure values, the heating transient part of the strain cycle is computed. Again, punch card residual strain data is output for subsequent calculations.

A typical set of input data for the chamber strain analysis is given in Appendix B. The particular data is for the transient heating condition (b), see Reference 1 for data card content and format.

Input for other conditions is similar to that listed in Appendix B.

For the RETSCP program, a secant modulus plasticity iteration, Reference 1, is performed within each run. Five such iterations were required for convergence of all elements with the bi-linear stress-strain curves. Total computing time for each run was 27 minutes on the IBM 7094 computer.

Results

A typical computed effective stress-effective strain diagram is shown in Figure 10 for a specific element; namely element 34, which is the element at the hot gas side surface beneath the rib, with temperature differences designated (864, 930, -300, -450) in Figure 5. Figure 10 depicts six strain loop calculations. The aforementioned effect of different pre-strain values on successive loop results is apparent. The net effect of strain hardening is automatically included by the use of cyclic-stress strain data. The important point is that a stable hysteresis loop is achieved which is representative of the strain range for that particular element on the twentieth cycle of thrust chember operation.

Referring to Figure 10, consider the detailed behavior of that particular element. Initial pre-cooling of the virgin material produces tensile yielding to the point (a). During the start transient, yielding occurs at a lower yield stress, point (b), corresponding to the elevated material temperature. The transient peak strain corresponds to point (c) on the curve.

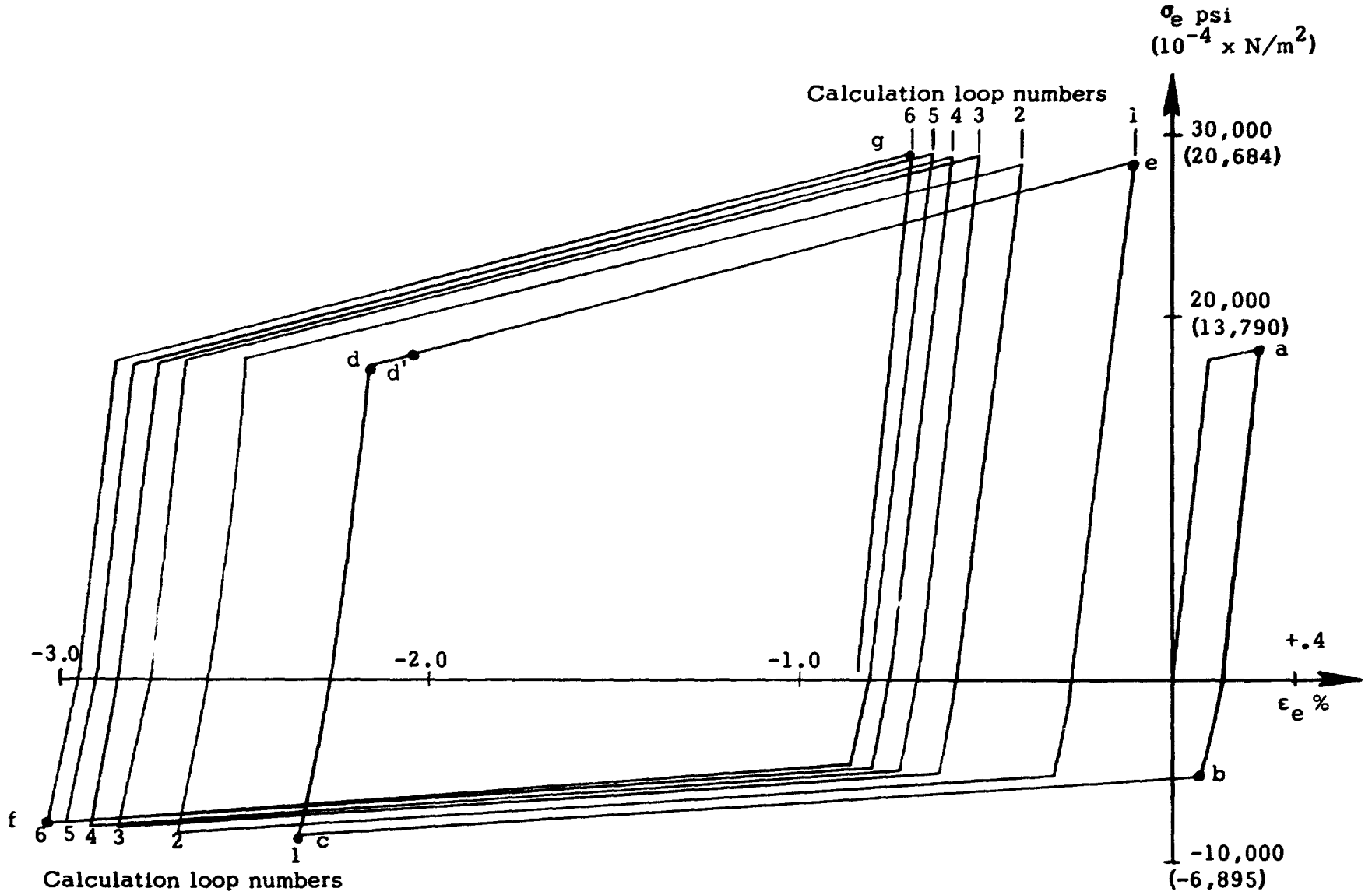

Figure 10. Typical calculated effective stress-effective strain diagram (Element 34)

Now, as the temperature difference is relaxed and steady state is achieved, the stress relaxes along the elastic line from (c) toward (d). In fact, for the particular element being examined, the strain relaxation is sufficient to produce a very slight amount of tensile yielding at the hot conditions (such as the point d'). The cooldown transient results in the tensile state, point (e). Cycling continues between these temperature limits; and, it is the magnitude of the stable strain range, such as between points (f) and (g), which will later be used to predict fatigue life.

Stress-strain cycles are shown in Figure 11, 12, and 13 for elements 15, 17, and 30 respectively. Behavior similar to element 34 can be identified. The convergence to a stable stress strain cycle is demonstrated in Figure 14. The peak strain values for each of the four elements 15, 17, 30, and 34 is plotted versus the calculation loop number. Note, that a constant value of strain range is approached for each element.

Sample output from the RETSCP program is given in Appendix C. Data from the hot and cold transient overshoots is given since these are limiting points of the strain cycle. The nodal point displacements (inches) and the yield data summary (inches/inch or psi where applicable) are given for both parts of the cycle.

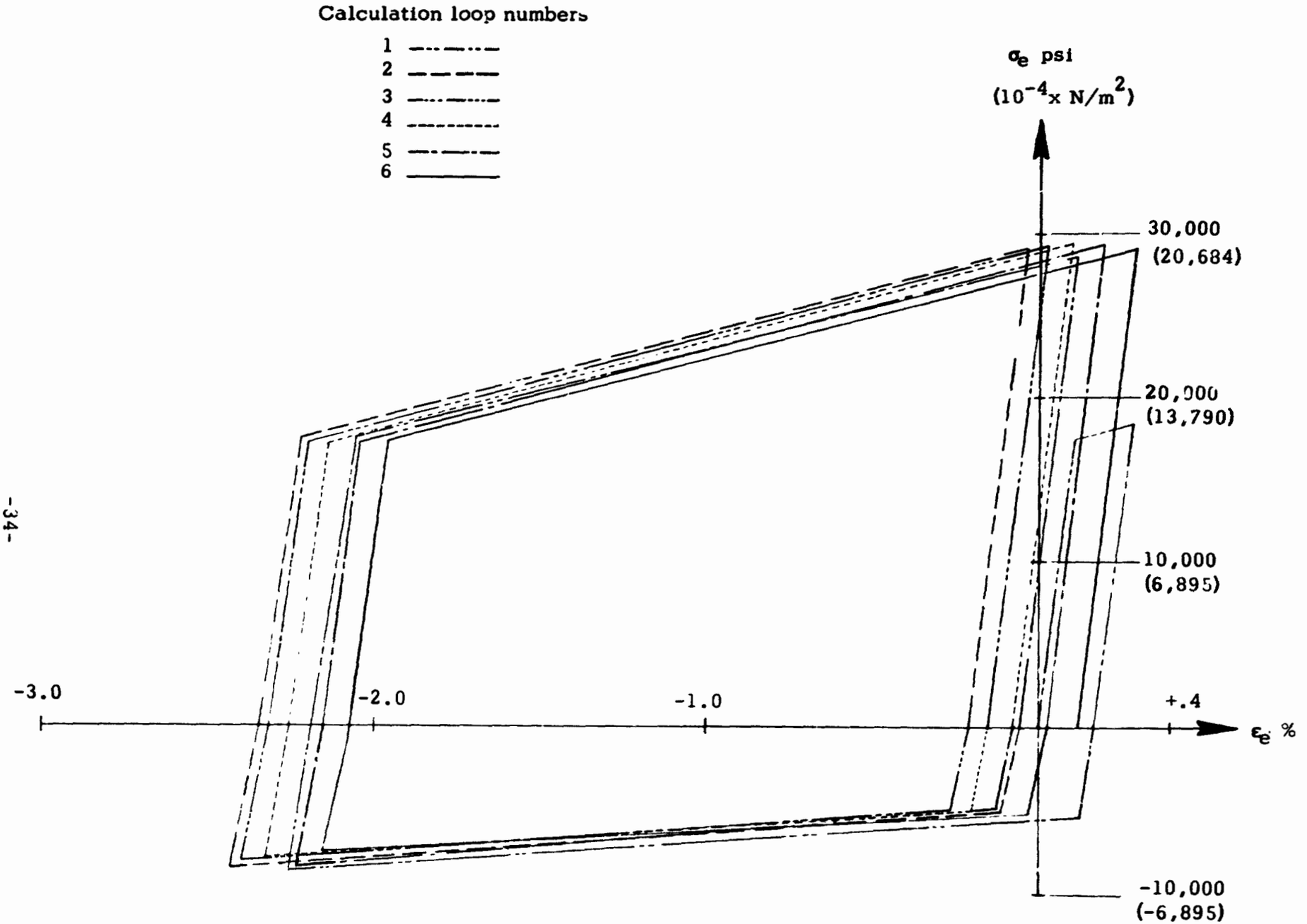

Figure 11. Effective stress-effective strain diagram for element 15.

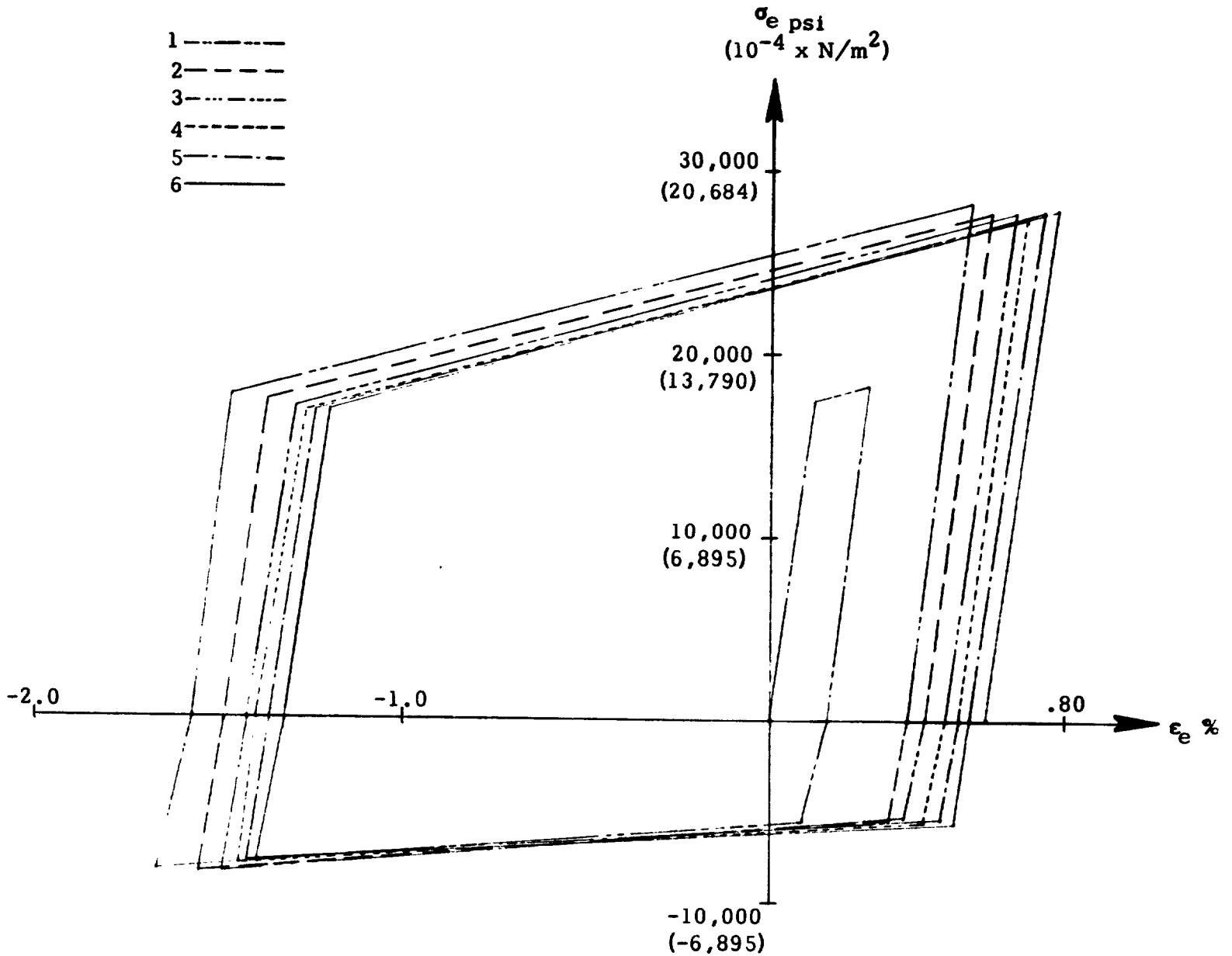

Figure 12. Effective stress-effective strain diagram for element 17.

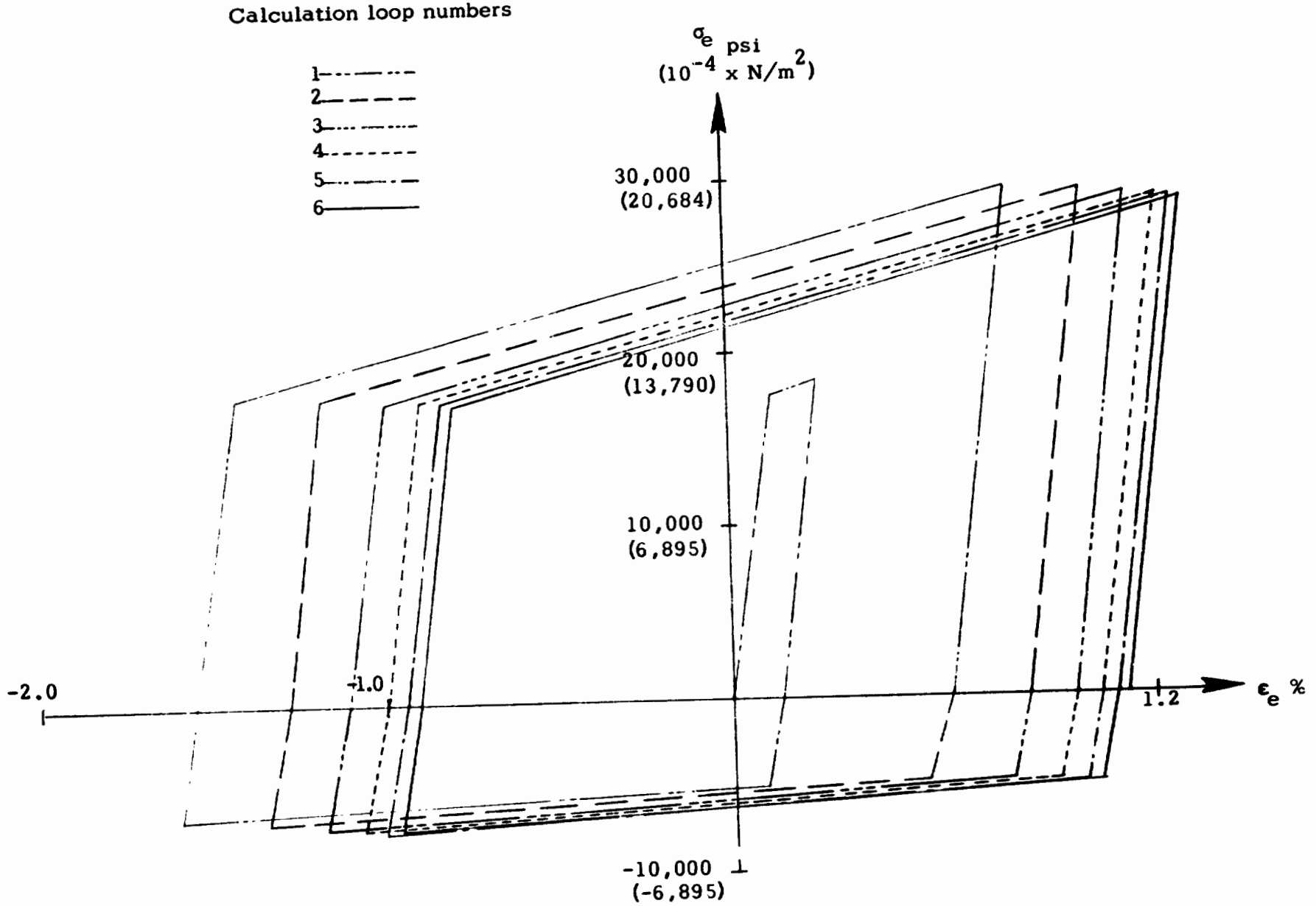

Figure 13. Effective stress-effective strain diagram for element 30.

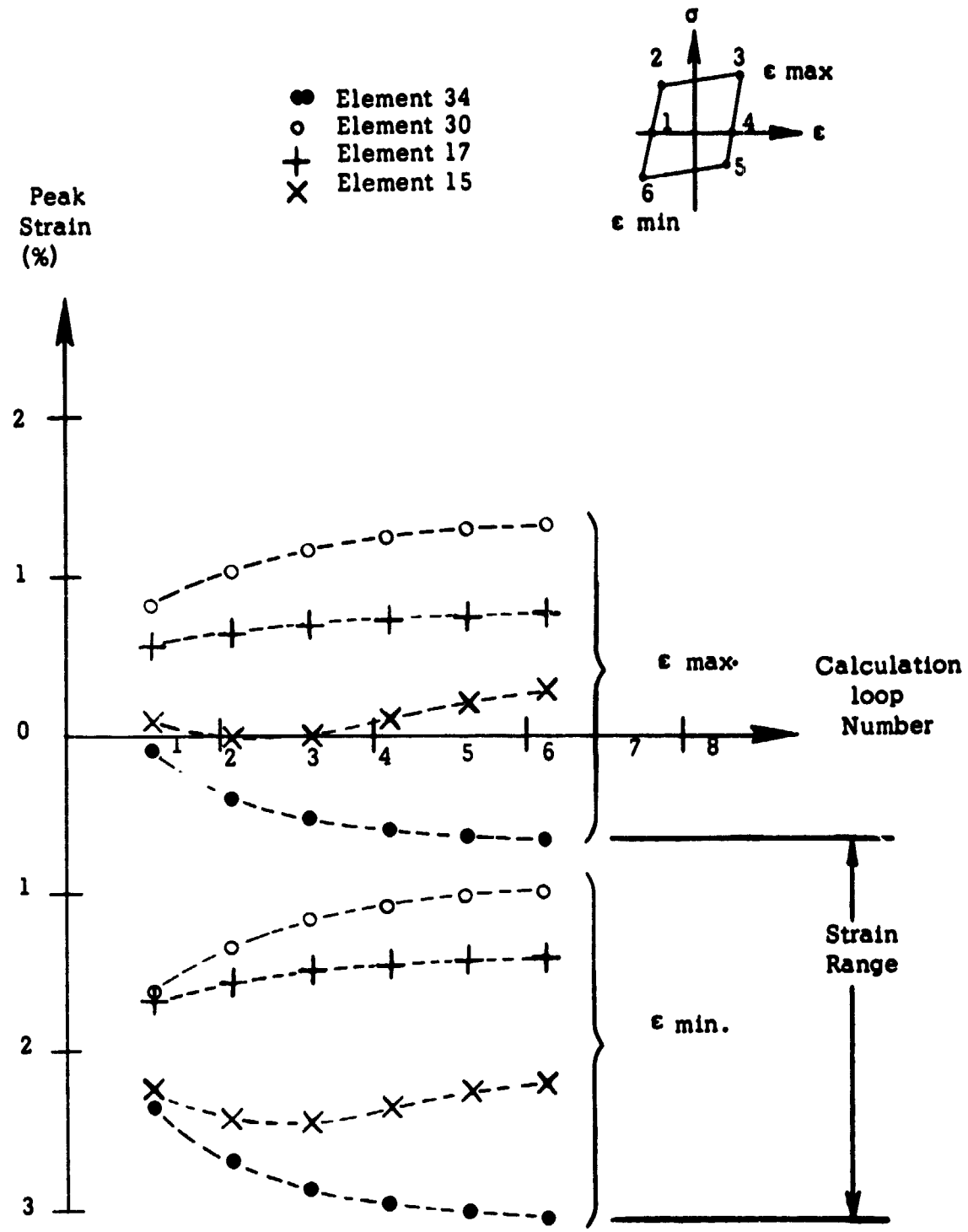

Figure 14. Strain range convergence.

The strain range is determined as follows: the difference between the total and plastic strains for the cooling cycle is the elastic strain, corresponding to the line 3-4 at the top of Figure 14. Thus, the effective strain range for the element, is the total strain from the heating half cycle 4-5-6, plus the cooling elastic strain 3-4.

The effective strain range distribution, at the combustion chamber nozzle throat, is presented in Figure 15. It is obvious that large strains in the copper liner are associated with regions of high temperatures. Also, as expected, the nickel closeout jacket behaves as an elastic structure.

Note, that the peak strain range location does not coincide with the peak temperature location. That is apparently due to the effect of coolant-to-chamber pressure differential. From elastic plate theory, pressure loading at run conditions would increase compression on the coolant side and relieve compression on the chamber side, along the line (i) - (ii) in Figure 15. Thus, the incompressibility of plastic strains increases the strain magnitudes toward the liner rib along the hot wall, point (iii) in Figure 15.

By extrapolation (cross plots of the strains at the element centers) to the hot wall surface, the maximum strain range is 2.46%, at point (iii) in Figure 15, where the maximum copper temperature is 970^{o}F (521^{o}C). Strain range values are generally between 2.0 and 2.5 percent throughout the hot portion of the copper liner.

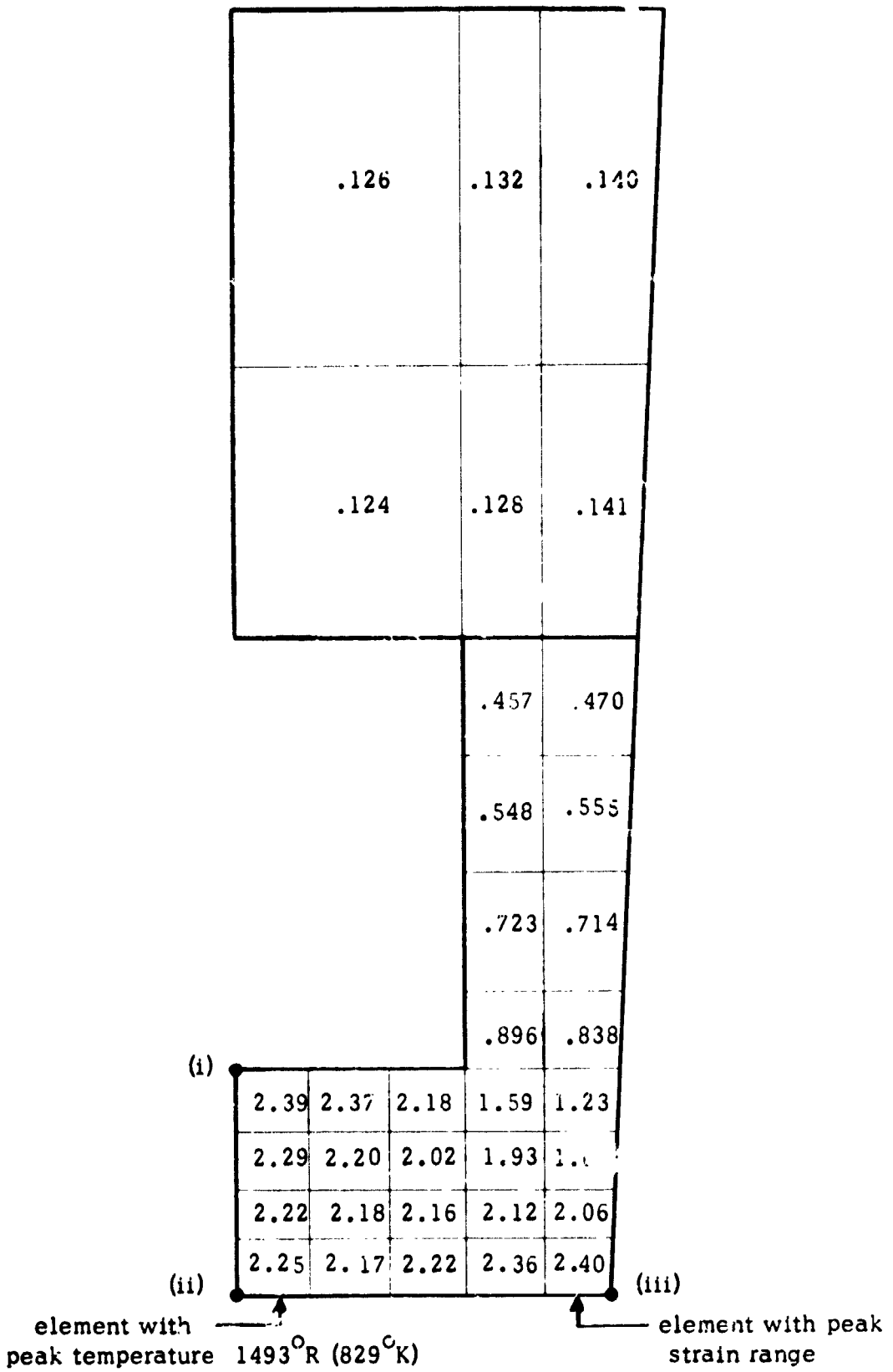

Figure 15. Effective strain range distribution (%) at nozzle throat.

The strain range results, which are the basis of the life estimate, depend on the extremes of the operating cycle. Intermediate points of the cycle may, in certain cases, be equally important in determining engine life. It was previously noted, that stress relaxation following the start transient, could lead to tensile hold strain under hot conditions. This phenomena is quite damaging according to the strain range partitioning method, Reference 14. Damage of this type is related to run time, Reference 19. For this particular case, run times are small (total accumulated run time less than 80 seconds) and the tensile hold strains are also small. Thus, the important point here is that the program has the ability to predict such hot tensile hold strains.

As an example, distributions of the hoop stress component within the copper are shown in Figure 16. The extremes of the cycle corresponding to the hot and cold transients are shown by the solid lines in Figure 16. Stress distributions at steady run conditions are indicated by the shaded area under the dash line curves. As anticipated, the stress relaxation is sufficient to produce hot tensile hold states.

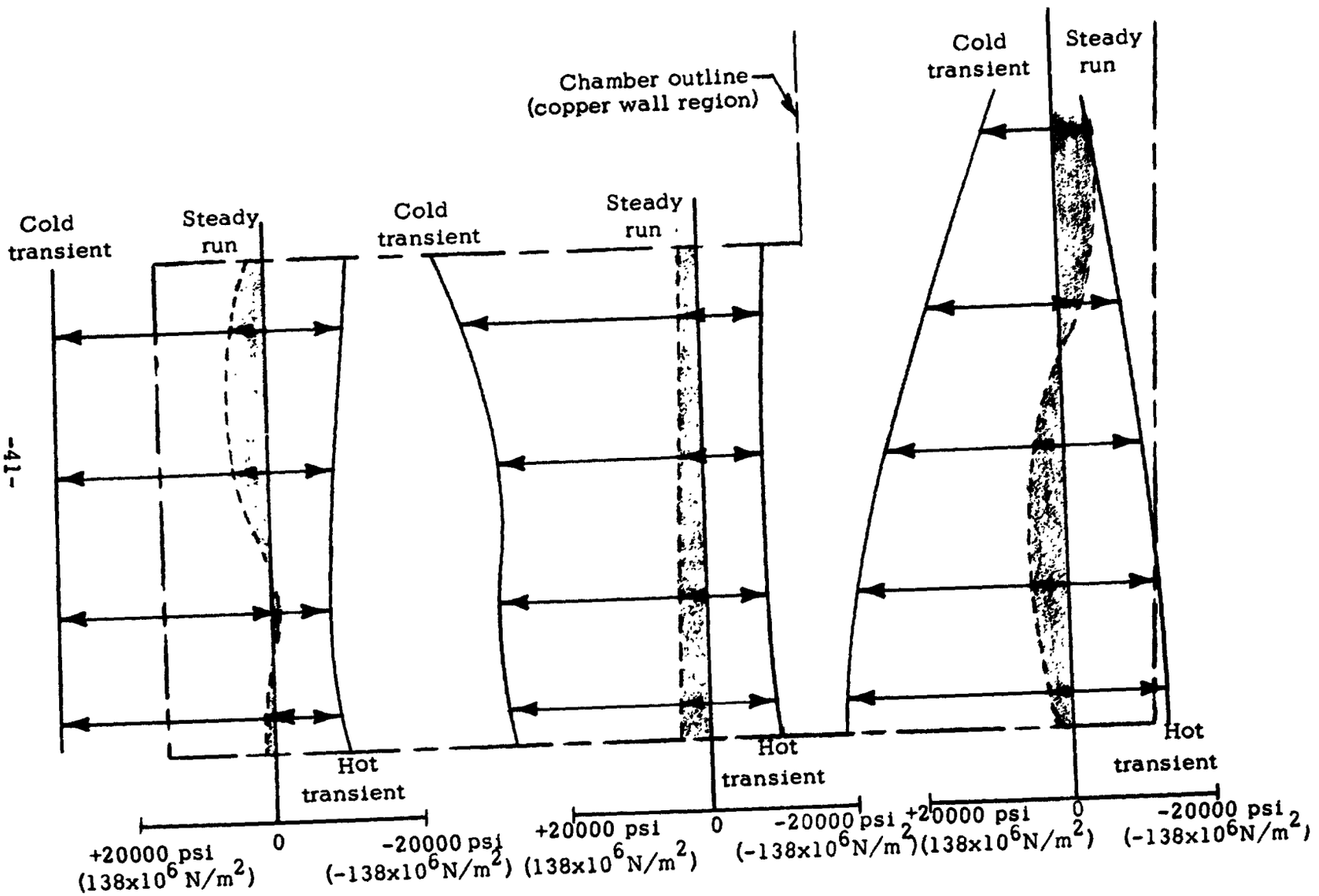

Figure 16. Hoop direction stress component distributions.

FATIGUE LIFE ANALYSIS

Prediction of chamber ... ue life is made by using the computed maximum effective strain range value in conjunction with uniaxial fatigue test data. A fatigue damage law is used to relate the actual operating cycle to uniaxial test conditions.

Material Properties

Typical low-cycle fatigue experimental data for OFHC copper, at room temperature is shown by the open circle in Figure 17, Reference 12. This data is compared with the well known Universal Slopes life predication (c.f. Reference 15); namely,

$$\Delta \epsilon_t = \frac{3.5\,\sigma_u}{E}\bar{N}_f^{-0.12} + \left[\ln\left(\frac{1}{1-RA}\right)\right]^{0.60}\bar{N}_f^{-0.60} \qquad (2)$$

where, the ultimate tensile strength (σ_u), modulus of elasticity (E) and reduction in area (RA) are based on the short term tensile test. The comparison not only shows the applicability of the Universal Slopes method; but, also indicates the degree of scatter which is associated with fatigue test results.

Now, for elevated test temperatures, the Universal Slopes prediction is modified, Reference 16. First, equation (2) is based on the short term properties at the elevated temperature. Then, to account for reduced life at elevated temperature, the "average" life is defined as one-fifth of the value in equation (2), $\bar{N}_f/5$. This procedure was based on comparison with a great deal of experimental data. Universal Slopes average life is compared, in Figure 17, with isothermal fatigue test data for OFHC copper at 1000°F (538°C).

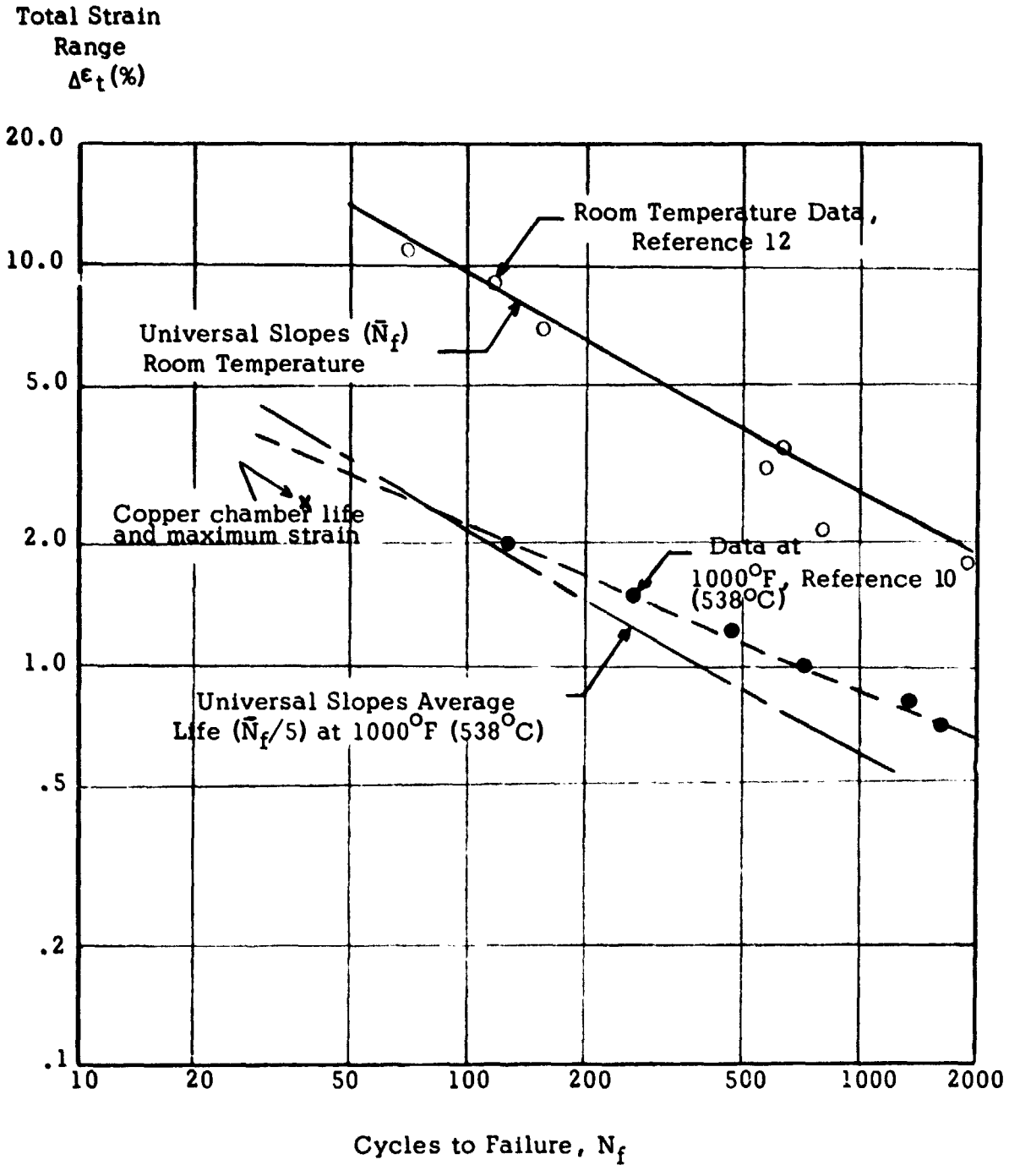

Figure 17. Isothermal fatigue of annealed OFHC copper.

The above sets of data are based on isothermal fatigue. That is, mechanically produced strain at a constant temperature. Thermal fatigue test data is obtained by thermal strain cycling between two temperature limits. This type of data was obtained for a zirconium-copper alloy, which was thermally cycled between 500°F (260°C) and 1000°F (538°C) Reference 17. For these conditions, fatigue life was lower than for isothermal testing at either of the temperature extremes. Other factors may have been involved in this life degradation. For the present work, the OFHC copper chamber fatigue life will be based on the 1000°F (538°C) data shown in Figure 17 (dash line curve).

Fatigue Damage

The linear cummulative damage law, Reference 2, is useful when the loading produces varying strain range values. According to that law, if n_j and n_k cycles are applied at conditions for which the fatigue life would be N_{f_j} and N_{f_k} respectively; then, the damage is accumulated linearly as follows:

$$D = \frac{n_j}{N_{f_j}} + \frac{n_k}{N_{f_k}} \tag{3}$$

Failure occurs when the cumulated damage totals unity.

For the case at hand, mean or typical loading conditions are assumed. Thus, the fatigue life is obtained directly from the material fatigue test data. Had the strain calculation been performed for various loading conditions; the life would be computed using equation (3). It was also

noted that, for the copper test chamber, experimental run times were small. Thus, creep or hold time effects are negligable. When this is not the case, a method for incorporating hold time effects, such as the strain range partitioning method, Reference 14, is employed.

Much work has been done in the area of fatigue damage, along both the experimental and analytical lines. The topic is touched on briefly here only to indicate how an accurate loading spectrum would be treated. Also, a precautionary remark is included, that engine firing hold time is critical to the operating life.

Results

Recall that the maximum value of effective strain range for the twentieth test cycle of the copper chamber was 2.46% at the hot wall centered under the rib. Based on the isothermal fatigue data at 1000°F (538°C), dash line in Figure 17, the predicted fatigue life for the copper chamber is 80 cycles. The point represented by the copper chamber life (39 cycles), and the maximum strain value for the twentieth cycle, is indicated by x in Figure 17.

CONCLUDING REMARKS

A detailed life analysis was conducted for a configuration and loading conditions which correspond directly to actual thrust chamber test conditions. In this manner a direct comparison of predicted and observed fatigue life is possible.

The analysis approximates the operating cycle by a succession of quasi-steady states. Thus, actual points within a cycle, and cycle to cycle variations can be identified. For example, this is the first known computation of tensile hold strain at hot engine test conditions. Hold time strain damage analysis was not performed since total hold time at steady state run conditions was less than 80 seconds for this particular chamber. However, for other configurations with longer test firings, hot tensile hold periods could be quite damaging as predicted by the strain range partitioning method.

The mathematical representation of the OFHC copper loading spectrum could be improved as follows: Calculate the strain-cycle at thermal conditions corresponding to the start and end of the test program; for example, cycles five and forty. Account for cycle by cycle strain hardening (isotropic or kinematic hardening) until hardening is sufficient that cyclic stress-strain data is applicable. Use the linear-cummulative damage law with the individual sets of strain data to predict life. Geometric changes such as coolant passage bulging, and the bulging effect on heat transfer, could also be included in such an analysis.

Finally, the full three-dimensional capabilities of the RETSCP program could be exploited. For example, axial curvature at the throat, with the resulting change in boundary constraint, could be modeled. Also, axial temperature distribution could be included. It is suspected that axial strain relief would be indicated by both of these three-dimensional phenomena.

It is the author's opinion that analytical refinements, such as those extended in this report and those proposed in the concluding remarks, not only produce more accurate life estimates; but also lead to greater understanding of the structural behavior of reusuable rocket engines.

APPENDIX A -- SYMBOLS

D	Fatigue damage fraction
E	Modulus of elasticity
m	Plastic modulus ratio
m_o	Plastic modulus ratio at reference temperature
$\bar{N}_f$	Universal slopes cycles to failure
N_f	Number of cycles to failure
p	Pressure
p_c	Chamber pressure
RA	Reduction in area
T	Temperature
t	Thrust chamber run time
x,y,z	Cartesian coordinates
$\Delta\epsilon_t$	Total strain range
ϵ_e	Strain (effective)
σ_e	Stress (effective)
σ_y	Yield stress
σ_o	Yield stress at reference temperature
ν	Poisson's ratio
λ_1	Yield stress slope with temperature $(\Delta\sigma_y/\Delta T)$
λ_2	Plastic modulus slope with temperature $(\Delta m/\Delta T)$

APPENDIX B --- SAMPLE RETSCP INPUT DATA

The following input listings are from the hot transient overshoot portion of the test cycle. The data are input from the sixth calculation loop. The data are included as programming guidelines. For complete description of input data and format see Reference 1.

UNUSED CORE 60455 THRU 64673

BEGIN EXECUTION.
9 102 34 102 3 3 30 2 5 1 1

1	0.	0.3400	0.
2	0.	0.3400	-0.0100
3	0.0440	0.3389	0.
4	0.0440	0.3389	-0.0100
5	0.0560	0.3386	0.
6	0.0560	0.3386	-0.0100
7	0.0859	0.3378	0.
8	0.0859	0.3378	-0.0100
9	0.	0.2300	0.
10	0.	0.2300	-0.0100
11	0.0440	0.2300	0.
12	0.0440	0.2300	-0.0100
13	0.0560	0.2300	0.
14	0.0560	0.2300	-0.0100
15	0.0801	0.2300	0.
16	0.0801	0.2300	-0.0100
17	0.	0.1500	0.
18	0.	0.1500	-0.0100
19	0.0440	0.1500	0.
20	0.0440	0.1500	-0.0100
21	0.0560	0.1500	0.
22	0.0560	0.1500	-0.0100
23	0.0759	0.1500	0.
24	0.0759	0.1500	-0.0100
25	0.0440	0.1100	0.
26	0.0440	0.1100	-0.0100
27	0.0560	0.1100	0.
28	0.0560	0.1100	-0.0100
29	0.0738	0.1100	0.
30	0.0738	0.1100	-0.0100
31	0.0440	0.0800	0.
32	0.0440	0.0800	-0.0100
33	0.0560	0.0800	0.
34	0.0560	0.0800	-0.0100
35	0.0722	0.0800	0.
36	0.0722	0.0800	-0.0100
37	0.0440	0.0500	0.
38	0.0440	0.0500	-0.0100
39	0.0560	0.0500	0.
40	0.0560	0.0500	-0.0100
41	0.0706	0.0500	0.
42	0.0706	0.0500	-0.0100
43	0.	0.0350	0.
44	0.	0.0350	-0.0100
45	0.0140	0.0350	0.
46	0.0140	0.0350	-0.0100
47	0.0290	0.0350	0.
48	0.0290	0.0350	-0.0100
49	0.0440	0.0350	0.
50	0.0440	0.0350	-0.0100
51	0.0560	0.0350	0.
52	0.0560	0.0350	-0.0100
53	0.0698	0.0350	0.
54	0.0698	0.0350	-0.0100
55	0.	0.0250	0.
56	0.	0.0250	-0.0100
57	0.0140	0.0250	0.
58	0.0140	0.0250	-0.0100

59	0.0290	0.0250	0.
60	0.0290	0.0250	-0.0100
61	0.0440	0.0250	0.
62	0.0440	0.0250	-0.0100
63	0.0560	0.0250	0.
64	0.0560	0.0250	-0.0100
65	0.0693	0.0250	0.
66	0.0693	0.0250	-0.0100
67	0.	0.0150	0.
68	0.	0.0150	-0.0100
69	0.0140	0.0150	0.
70	0.0140	0.0150	-0.0100
71	0.0290	0.0150	0.
72	0.0290	0.0150	-0.0100
73	0.0440	0.0150	0.
74	0.0440	0.0150	-0.0100
75	0.0560	0.0150	0.
76	0.0560	0.0150	-0.0100
77	0.0688	0.0150	0.
78	0.0688	0.0150	-0.0100
79	0.	0.0050	0.
80	0.	0.0050	-0.0100
81	0.0140	0.0050	0.
82	0.0140	0.0050	-0.0100
83	0.0290	0.0050	0.
84	0.0290	0.0050	-0.0100
85	0.0440	0.0050	0.
86	0.0440	0.0050	-0.0100
87	0.0560	0.0050	0.
88	0.0560	0.0050	-0.0100
89	0.0683	0.0050	0.
90	0.0683	0.0050	-0.0100
91	0.	0.	0.
92	0.	0.	-0.0100
93	0.0140	-0.0004	0.
94	0.0140	-0.0004	-0.0100
95	0.0290	-0.0008	0.
96	0.0290	-0.0008	-0.0100
97	0.0440	-0.0012	0.
98	0.0440	-0.0012	-0.0100
99	0.0560	-0.0015	0.
100	0.0560	-0.0015	-0.0100
101	0.0680	-0.0018	0.
102	0.0680	-0.0018	-0.0100

1	3	1	8	
1	6	9	16	
4	10	17	30	
9	14	31	42	
13	19	43	54	
15	24	55	66	
20	29	67	78	
25	34	79	90	
30	34	91	102	

1	55000.0000	0.	1.0000	0.
1	30000000.0000	0.3100	7.2000	
2	9200.0000	4.6300	41.7000	33.1000
2	10000300.0000	0.3300	9.8000	
3	6000.0000	2.6300	117.7000	6.3200
3	10000000.0000	0.3300	9.8000	

1	-0.	0.	0.

2	-0.	0.	0.
3	-0.	0.	0.
4	0.	-0.	-0.
5	-0.	-0.	0.
6	-0.	-0.	0.
7	-0.24119800	0.20361870	0.03757928
8	-0.20024025	0.16321322	0.03702705
9	-0.46199599	0.40736733	0.05462863
10	-0.51167550	0.46574701	0.04592849
11	-0.57119052	0.53509711	0.03609341
12	-0.59211117	0.56452720	0.02758399
13	-0.55684035	0.54027962	0.01656076
14	-0.44458096	0.43231229	0.01226866
15	0.03955957	-0.12612113	0.08656155
16	0.35231858	-0.43870473	0.08638617
17	0.21659513	-0.28870822	0.07211310
18	-0.29719573	0.22219253	0.07500317
19	-0.29988073	0.24818914	0.05169158
20	0.53768418	-0.62040551	0.08272132
21	0.30823641	-0.38345495	0.07521857
22	-0.20431232	0.12749442	0.07681786
23	-0.33050895	0.25675409	0.07375488
24	-0.31761079	0.24893337	0.06867746
25	0.87380560	-0.94867547	0.07486983
26	0.32188795	-0.39747562	0.07558767
27	-0.24484736	0.16981211	0.07503523
28	-0.50939558	0.43244885	0.07694674
29	-0.52636082	0.45367645	0.07268438
30	1.02155843	-1.09425323	0.07269479
31	0.39731283	-0.47014479	0.07283194
32	-0.25578052	0.18081336	0.07496706
33	-0.59632719	0.51974344	0.07658371
34	-0.73569323	0.65962893	0.07606427

2	4	12	10	1	3	11	9	1	-153.000
4	6	14	12	3	5	13	11	1	-153.000
6	8	16	14	5	7	15	13	1	-153.000
10	12	20	18	9	11	19	17	1	-30.000
12	14	22	20	11	13	21	19	1	18.000
14	16	24	22	13	15	23	21	1	37.000
20	22	28	26	19	21	27	25	3	235.000
22	24	30	28	21	23	29	27	3	249.000
26	28	34	32	25	27	33	31	3	316.000
28	30	36	34	27	29	35	33	3	327.000
32	34	40	38	31	33	39	37	2	483.000
34	36	42	40	33	35	41	39	2	493.000
38	40	52	50	37	39	51	49	2	601.000
40	42	54	52	39	41	53	51	2	606.000
44	46	58	56	43	45	57	55	2	830.000
46	48	60	58	45	47	59	57	2	814.000
48	50	62	60	47	49	61	59	2	776.000
50	52	64	62	49	51	63	61	2	727.000
52	54	66	64	51	53	65	63	2	708.000
56	58	70	68	55	57	69	67	2	847.000
58	60	72	70	57	59	71	69	2	839.000
60	62	74	72	59	61	73	71	2	799.000
62	64	76	74	61	63	75	73	2	753.000
64	66	78	76	63	65	77	75	2	743.000
68	70	82	80	67	69	81	79	2	885.000
70	72	84	82	69	71	83	81	2	878.000
72	74	86	84	71	73	85	83	2	846.000

74	76	88	86	73	75	87	85	2	817.000
76	78	90	88	75	77	89	87	2	809.000
80	82	94	92	79	81	93	91	2	931.000
82	84	96	94	81	83	95	93	2	912.000
84	86	98	96	83	85	97	95	2	896.000
86	88	100	98	85	87	99	97	2	876.000
88	90	102	100	87	89	101	99	2	864.000

1	0	1	0	0.	0.	0.	-0.
2	0	1	0	-0.	-0.	0.00000615	-0.
3	1	1	0	0.	0.	0.	-0.
4	1	1	0	-0.	-0.	0.00000615	-0.
5	1	1	0	0.	0.	0.	-0.
6	1	1	0	-0.	-0.	0.00000615	-0.
7	0	1	0	0.	0.	0.	-3.00000000
8	0	1	0	-0.	-0.	0.00000615	-3.00000000
9	0	1	0	0.	0.	0.	-0.
10	0	1	0	-0.	-0.	0.00000615	-0.
11	1	1	0	0.	0.	0.	-0.
12	1	1	0	-0.	-0.	0.00000615	-0.
13	1	1	0	0.	0.	0.	-0.
14	1	1	0	0.	-0.	0.00000615	-0.
15	0	1	0	0.	0.	0.	-3.00000000
16	0	1	0	0.	0.	0.00000615	-3.00000000
17	0	1	0	0.	0.	0.	-0.
18	0	1	0	-0.	-0.	0.00000615	-0.
19	1	1	0	0.	0.	0.	-0.
20	1	1	0	-0.	-0.	0.00000615	-0.
21	1	1	0	0.	0.	0.	-0.
22	1	1	0	-0.	-0.	0.00000615	-0.
23	0	1	0	0.	0.	0.	-3.00000000
24	0	1	0	0.	0.	0.00000615	-3.00000000
25	1	1	0	0.	0.	0.	-0.
26	1	1	0	-0.	-0.	0.00000615	-0.
27	1	1	0	0.	0.	0.	-0.
28	1	1	0	-0.	-0.	0.00000615	-0.
29	0	1	0	0.	0.	0.	-3.00000000
30	0	1	0	-0.	-0.	0.00000615	-3.00000000
31	1	1	0	0.	0.	0.	-0.
32	1	1	0	-0.	-0.	0.00000615	-0.
33	1	1	0	0.	0.	0.	-0.
34	1	1	0	-0.	-0.	0. 0000615	-0.
35	0	1	0	0.	0.	0.	-3.00000000
36	0	1	0	-0.	-0.	0.00000615	-3.00000000
37	1	1	0	0.	0.	0.	-0.
38	1	1	0	-0.	-0.	0.00000615	-0.
39	1	1	0	0.	0.	0.	-0.
40	1	1	0	-0.	-0.	0.00000615	-0.
41	0	1	0	0.	0.	0.	-3.00000000
42	0	1	0	-0.	-0.	0.00000615	-3.00000000
43	0	1	0	0.	0.	0.	-0.
44	0	1	0	-0.	-0.	0.00000615	-0.
45	1	1	0	0.	0.	0.	-0.
46	1	1	0	-0.	-0.	0.00000615	-0.
47	1	1	0	0.	0.	0.	-0.
48	1	1	0	-0.	-0.	0.00000615	-0.
49	1	1	0	0.	0.	0.	-0.
50	1	1	0	-0.	-0.	0.00000615	-0.
51	1	1	0	0.	0.	0.	-0.
52	1	1	0	-0.	-0.	0.00000615	-0.
53	0	1	0	0.	0.	0.	-3.00000000

54	0	1	0	-0.	-0.	0.00000615	-3.00000000
55	0	1	0	0.	0.	0.	-0.
56	0	1	0	-0.	-0.	0.00000615	-0.
57	1	1	0	0.	0.	0.	-0.
58	1	1	0	-0.	-0.	0.00000615	-0.
59	1	1	0	0.	0.	0.	-0.
60	1	1	0	-0.	-0.	0.00000615	-0.
61	1	1	0	0.	0.	0.	-0.
62	1	1	0	-0.	-0.	0.00000615	-0.
63	1	1	0	0.	0.	0.	-0.
64	1	1	0	-0.	-0.	0.00000615	-0.
65	0	1	0	0.	0.	0.	-3.00000000
66	0	1	0	-0.	-0.	0.00000615	-3.00000000
67	0	1	0	0.	0.	0.	-0.
68	0	1	0	-0.	-0.	0.00000615	-0.
69	1	1	0	0.	0.	0.	-0.
70	1	1	0	-0.	-0.	0.00000615	-0.
71	1	1	0	0.	0.	0.	-0.
72	1	1	0	-0.	-0.	0.00000615	-0.
73	1	1	0	0.	0.	0.	-0.
74	1	1	0	-0.	-0.	0.00000615	-0.
75	1	1	0	0.	0.	0.	-0.
76	1	1	0	-0.	-0.	0.00000615	-0.
77	0	1	0	0.	0.	0.	-3.00000000
78	0	1	0	0.	0.	0.00000615	-3.00000000
79	0	1	0	0.	0.	0.	-0.
80	0	1	0	-0.	-0.	0.00000615	-0.
81	1	1	0	0.	0.	0.	-0.
82	1	1	0	-0.	-0.	0.00000615	-0.
83	1	1	0	0.	0.	0.	-0.
84	1	1	0	-0.	-0.	0.00000615	-0.
85	1	1	0	0.	0.	0.	-0.
86	1	1	0	-0.	-0.	0.00000615	-0.
87	1	1	0	0.	0.	0.	-0.
88	1	1	0	-0.	-0.	0.00000615	-0.
89	0	1	0	0.	0.	0.	-3.00000000
90	0	1	0	0.	0.	0.00000 '5	-3.00000000
91	0	1	0	0.	0.	0.	-0.
92	0	1	0	0.	-0.	0.00000615	-0.
93	1	1	0	0.	0.	0.	-0.
94	1	1	0	-0.	-0.	0.00000615	-0.
95	1	1	0	0.	0.	0.	-0.
96	1	1	0	-0.	-0.	0.00000615	-0.
97	1	1	0	0.	0.	0.	-0.
98	1	1	0	-0.	-0.	0.00000615	-0.
99	1	1	0	0.	0.	0.	-0.
100	1	1	0	-0.	-0.	0.00000615	-0.
101	0	1	0	0.	0.	0.	-3.00000000
102	0	1	0	0.	0.	0.00000615	-3.00000000

17	0.	0.1150	-0.
18	0.	0.1150	-0.
19	0.1045	0.1150	-0.
20	0.1045	0.1150	-0.
25	0.1829	0.	-0.
26	0.1829	0.	-0.
31	0.1568	0.	-0.
32	0.1568	0.	-0.
37	0.0915	0.	-0.
38	0.0915	0.	-0.
43	0.	-0.0366	-0.

44	0.	-0.0366	-0.
45	0.	-0.0785	-0.
46	0.	-0.0785	-0.
47	0.	-0.0785	-0.
48	0.	-0.0785	-0.
49	0.0392	-0.0392	-0.
50	0.0392	-0.0392	-0.
91	0.	0.0130	-0.
92	0.	0.0130	-0.
93	0.	0.0260	-0.
94	0.	0.0260	-0.
95	0.	0.0260	-0.
96	0.	0.0260	-0.
97	0.	0.0234	-0.
98	0.	0.0234	-0.
99	0.	0.0208	-0.
100	0.	0.0208	-0.
101	0.	0.0104	-0.
102	0.	0.0104	-0.

APPENDIX C --- SAMPLE RETSCP OUTPUT DATA

The following data from the hot and cold transient overshoots is given since these are limiting points of the strain cycle. The nodal point displacements (inches) and the yield data summary (inches/inch or psi where applicable) are given for both parts of the cycle.

Hot Transient Overshoot - Condition (b) - Sixth Calculation Loop.

NODE	X-DISPLACEMENTS	Y-DISPLACEMENTS	Z-DISPLACEMENTS
1	-0.	-0.88608476E-03	0.
2	0.	-0.88608467E-03	0.61600000E-05
3	-0.23587382E-04	-0.88179445E-03	0.
4	-0.23587379E-04	-0.88179429E-03	0.61600000E-05
5	-0.30502287E-04	-0.89116723E-03	0.
6	-0.30502289E-04	-0.89116712E-03	0.61600000E-05
7	-0.46498187E-04	-0.88723857E-03	0.
8	-0.46498179E-04	-0.88723844E-03	0.61600000E-05
9	-0.	-0.71461207E-03	0.
10	0.	-0.71461216E-03	0.61600000E-05
11	-0.25054049E-04	-0.71488000E-03	0.
12	-0.25054048E-04	-0.71488013E-03	0.61600000E-05
13	-0.29606212E-04	-0.70346694E-03	0.
14	-0.29606210E-04	-0.70346705E-03	0.61600000E-05
15	-0.37009233E-04	-0.70617849E-03	0.
16	-0.37009240E-04	-0.70617862E-03	0.61600000E-05
17	-0.	-0.72652270E-03	0.
18	0.	-0.72652262E-03	0.61600000E-05
19	-0.41415733E-04	-0.74144433E-03	0.
20	-0.41415734E-04	-0.74144416E-03	0.61600000E-05
21	-0.43175319E-04	-0.76064608E-03	0.
22	-0.43175324E-04	-0.76064599E-03	0.61600000E-05
23	-0.39993184E-04	-0.76311568E-03	0.
24	-0.39993176E-04	-0.76311554E-03	0.61600000E-05
25	-0.84012336E-04	-0.10265325E-02	0.
26	-0.84012296E-04	-0.10265327E-02	0.61600000E-05
27	-0.75818070E-04	-0.10258310E-02	0.
28	-0.75818058E-04	-0.10258311E-02	0.61600000E-05
29	-0.54283927E-04	-0.10357994E-02	0.
30	-0.54283930E-04	-0.10357994E-02	0.61600000E-05
31	-0.69739825E-04	-0.12962886E-02	0.
32	-0.69739796E-04	-0.12962885E-02	0.61600000E-05
33	-0.67687368E-04	-0.13071462E-02	0.
34	-0.67687371E-04	-0.13071462E-02	0.61600000E-05
35	-0.69035191E-04	-0.13172704E-02	0.
36	-0.69035190E-04	-0.13172704E-02	0.61600000E-05
37	-0.15328293E-03	-0.17001834E-02	0.
38	-0.15328269E-03	-0.17001836E-02	0.61600000E-05
39	-0.13167387E-03	-0.17144089E-02	0.
40	-0.13167381E-03	-0.17144090E-02	0.61600000E-05
41	-0.90028589E-04	-0.17178484E-02	0.
42	-0.90028589E-04	-0.17178484E-02	0.61600000E-05
43	-0.	-0.24610800E-02	0.
44	-0.	-0.24610844E-02	0.61600000E-05
45	0.10397403E-03	-0.24080224E-02	0.
46	-0.10397429E-03	-0.24080249E-02	0.61600000E-05
47	-0.14351028E-03	-0.22412936E-02	0.
48	-0.14350806E-03	-0.22412971E-02	0.61600000E-05
49	-0.14712982E-03	-0.19827386E-02	0.
50	-0.14713000E-03	-0.19827397E-02	0.61600000E-05
51	-0.14346524E-03	-0.19413932E-02	0.
52	-0.14346534E-03	-0.19413934E-02	0.61600000E-05
53	-0.10171195E-03	-0.19407803E-02	0.
54	-0.10171198E-03	-0.19407809E-02	0.61600000E-05
55	-0.	-0.27589332E-02	0.

56	0.	-0.27589342E-02	0.61600000E-05
57	-0.14961475E-04	-0.26815209E-02	0.
58	-0.14961760E-04	-0.26815216E-02	0.61600000E-05
59	-0.13278892E-04	-0.24702880E-02	0.
60	-0.13278252E-04	-0.24702892E-02	0.61600000E-05
61	-0.52607844E-04	-0.22390910E-02	0.
62	-0.52608622E-04	-0.22390918E-02	0.61600000E-05
63	-0.10137519E-03	-0.21518315E-02	0.
64	-0.10137531E-03	-0.21518316E-02	0.61600000E-05
65	-0.11133646E-03	-0.21244269E-02	0.
66	-0.11133650E-03	-0.21244277E-02	0.61600000E-05
67	-0.	-0.29875714E-02	0.
68	0.	-0.29875707E-02	0.61600000E-05
69	0.69831814E-04	-0.29112592E-02	0.
70	0.69831111E-04	-0.29112595E-02	0.61600000E-05
71	0.82061066E-04	-0.27249408E-02	0.
72	0.82061051E-04	-0.27249421E-02	0.61600000E-05
73	0.15795580E-04	-0.25248605E-02	0.
74	0.15795216E-04	-0.25248627E-02	0.61600000E-05
75	-0.57424884E-04	-0.24108064E-02	0.
76	-0.57425292E-04	-0.24108058E-02	0.61600000E-05
77	-0.12381681E-03	-0.23625663E-02	0.
78	-0.12381691E-03	-0.23625683E-02	0.61600000E-05
79	-0.	-0.31631419E-02	0.
80	0.	-0.31631408E-02	0.61600000E-05
81	0.11823433E-03	-0.31231233E-02	0.
82	0.11823412E-03	-0.31231252E-02	0.61600000E-05
83	0.15258963E-03	-0.29992765E-02	0.
84	0.15258970E-03	-0.29992779E-02	0.61600000E-05
85	0.85244905E-04	-0.28376625E-02	0.
86	0.85245527E-04	-0.28376662E-02	0.61600000E-05
87	-0.19475119E-04	-0.27270142E-02	0.
88	-0.19474595E-04	-0.27270131E-02	0.61600000E-05
89	-0.14010049E-03	-0.26732775E-02	0.
90	-0.14010062E-03	-0.26732800E-02	0.61600000E-05
91	-0.	-0.32487792E-02	0.
92	0.	-0.32487779E-02	0.61600000E-05
93	0.13040668E-03	-0.32313835E-02	0.
94	0.13040627E-03	-0.32313852E-02	0.61600000E-05
95	0.18750193E-03	-0.31593302E-02	0.
96	0.18750230E-03	-0.31593305E-02	0.61600000E-05
97	0.12840016E-03	-0.30462444E-02	0.
98	0.12840173E-03	-0.30462472E-02	0.61600000E-05
99	0.80950471E-05	-0.29660175E-02	0.
100	0.80953512E-05	-0.29660157E-02	0.61600000E-05
101	-0.15344502E-03	-0.29279065E-02	0.
102	-0.15344513E-03	-0.29279085E-02	0.61600000E-05

Hot Transient Overshoot - Condition (b) - Sixth Calculation Loop.

YIELD CHECK AFTER 5 ITTERATIONS

ELEMENT	TOTAL STRAIN	PLASTIC STRAIN	EFFECTIVE STRESS	YIELD STRESS	SECANT MODULUS	SECANT POISSON
1	0.000736	0.	22066.5	55000.0	30000000.0	0.3100
2	0.000835	0.	25055.5	55000.0	30000000.0	0.3100
3	0.000909	0.	27271.1	55000.0	30000000.0	0.3100
4	0.000714	0.	21434.0	55000.0	30000000.0	0.3100
5	0.000777	0.	23295.7	55000.0	30000000.0	0.3100
6	0.000887	0.	26596.0	55000.0	30000000.0	0.3100
7	0.003507	0.002624	8832.3	5381.9	2518365.1	0.4572
8	0.003629	0.002736	8939.2	5345.1	2462951.8	0.4581
9	0.004294	0.003340	9539.6	5168.9	2221407.8	0.4622
10	0.004344	0.003387	9568.6	5140.0	2202772.5	0.4626
11	0.005823	0.004995	8281.9	6963.7	1422300.7	0.4758
12	0.005723	0.004904	8194.5	6917.4	1431760.6	0.4757
13	0.007314	0.006526	7872.3	6417.4	1076385.1	0.4817
14	0.006828	0.006055	7733.6	6394.2	1132568.8	0.4807
15	0.022099	0.021257	8425.0	5357.1	381230.5	0.4935
16	0.021964	0.021105	8592.2	5431.2	391193.4	0.4933
17	0.020107	0.019233	8737.3	5607.1	434547.3	0.4926
18	0.014359	0.013533	8263.5	5834.0	575485.5	0.4902
19	0.010888	0.010108	7802.6	5922.0	716592.9	0.4878
20	0.021170	0.020360	8099.0	5278.4	382565.3	0.4935
21	0.020285	0.019479	8067.0	5315.4	397672.8	0.4932
22	0.018560	0.017736	8247.8	5500.6	444373.1	0.4924
23	0.017662	0.016804	8580.7	5713.6	485824.9	0.4917
24	0.015213	0.014387	8263.8	5759.9	543205.8	0.4908
25	0.020482	0.019723	7580.2	5102.5	370098.8	0.4937
26	0.020117	0.019356	7612.4	5134.9	378401.6	0.4936
27	0.019873	0.019080	7932.8	5283.0	399167.9	0.4932
28	0.019557	0.018736	8204.4	5417.3	419514.4	0.4929
29	0.018970	0.018149	8203.6	5454.3	432460.6	0.4926
30	0.020753	0.020043	7095.0	4889.5	341881.7	0.4942
31	0.020032	0.019309	[illegible]5.4	4977.4	360743.6	0.4939
32	0.020490	0.019745	7458.2	5051.5	363986.9	0.4938
33	0.021864	0.021079	7856.5	5144.1	359328.0	0.4939
34	0.022242	0.021437	8045.6	5199.7	361732.6	0.4939

Cold Transient Overshoot - Condition (d) - Sixth Calculation Loop.

NODE	X-DISPLACEMENTS	Y-DISPLACEMENTS	Z-DISPLACEMENTS
1	-0.	-0.23490101E-02	0.
2	0.	-0.23490102E-02	0.10780000E-04
3	-0.62681047E-04	-0.23511011E-02	0.
4	-0.62681044E-04	-0.23511010E-02	0.10780000E-04
5	-0.80041566E-04	-0.23502476E-02	0.
6	-0.80041566E-04	-0.23502477E-02	0.10780000E-04
7	-0.12306707E-03	-0.23486421E-02	0.
8	-0.12306707E-03	-0.23486420E-02	0.10780000E-04
9	-0.	-0.22777465E-02	0.
10	0.	-0.22777464E-02	0.10780000E-04
11	-0.66755759E-04	-0.22733267E-02	0.
12	-0.66755758E-04	-0.22733267E-02	0.10780000E-04
13	-0.84035568E-04	-0.22735915E-02	0.
14	-0.84035571E-04	-0.22735915E-02	0.10780000E-04
15	-0.11913780E-03	-0.22732855E-02	0.
16	-0.11913781E-03	-0.22732856E-02	0.10780000E-04
17	-0.	-0.21244456E-02	0.
18	0.	-0.21244456E-02	0.10780000E-04
19	-0.55227523E-04	-0.21291690E-02	0.
20	-0.55227521E-04	-0.21291680E-02	0.10780000E-04
21	-0.76546202E-04	-0.21263552E-02	0.
22	-0.76546158E-04	-0.21263551E-02	0.10780000E-04
23	-0.11135168E-03	-0.21247174E-02	0.
24	-0.11135166E-03	-0.21247173E-02	0.10780000E-04
25	0.13862845E-03	-0.21229360E-02	0.
26	0.13862844E-03	-0.21229361E-02	0.10780000E-04
27	0.34047618E-04	-0.20815265E-02	0.
28	0.34047622E-04	-0.20815266E-02	0.10780000E-04
29	-0.10866480E-03	-0.20734486E-02	0.
30	-0.10866481E-03	-0.20734487E-02	0.10780000E-04
31	0.15854322E-03	-0.21555454E-02	0.
32	0.15854326E-03	-0.21555453E-02	0.10780000E-04
33	0.55852819E-04	-0.21565731E-02	0.
34	0.55852801E-04	-0.21565729E-02	0.10780000E-04
35	-0.11307176E-03	-0.21575385E-02	0.
36	-0.11307176E-03	-0.21575385E-02	0.10780000E-04
37	0.16640211E-03	-0.22342872E-02	0.
38	0.16640323E-03	-0.22342874E-02	0.10780000E-04
39	0.25685849E-04	-0.22582630E-02	0.
40	0.25685863E-04	-0.22582632E-02	0.10780000E-04
41	-0.11905513E-03	-0.22717080E-02	0.
42	-0.11905514E-03	-0.22717081E-02	0.10780000E-04
43	-0.	-0.26555197E-02	0.
44	0.	-0.26555205E-02	0.10780000E-04
45	-0.42558512E-04	-0.26059449E-02	0.
46	-0.42558233E-04	-0.26059464E-02	0.10780000E-04
47	-0.10646669E-04	-0.24966272E-02	0.
48	-0.10647433E-04	-0.24966285E-02	0.10780000E-04
49	0.64366679E-04	-0.22894134E-02	0.
50	0.64366715E-04	-0.22894129E-02	0.10780000E-04
51	-0.25685194E-04	-0.22863830E-02	0.
52	-0.25685205E-04	-0.22863832E-02	0.10780000E-04
53	-0.12056132E-03	-0.23004479E-02	0.
54	-0.12056132E-03	-0.23004478E-02	0.10780000E-04
55	-0.	-0.25970245E-02	0.

56	0.	-0.25970243E-02	0.10780000E-04
57	0.30925059E-04	-0.25427761E-02	C.
58	0.30925301E-04	-0.25427763E-02	C.10780000E-04
59	0.69855956E-04	-0.23828126E-02	C.
60	0.69855887E-04	-0.23828132E-02	C.10780000E-04
61	0.55957443E-05	-0.22707196E-02	C.
62	0.55957371E-05	-0.22707189E-02	C.10780000E-04
63	-0.45624547E-04	-0.22860422E-02	C.
64	-0.45624562E-04	-0.22860427E-02	C.10780000E-04
65	-0.12021014E-03	-0.22937470E-02	C.
66	-0.12021014E-03	-0.22937468E-02	C.10780000E-04
67	-0.	-0.24871169E-02	C.
68	0.	-0.24871161E-02	C.10780000E-04
69	0.94635975E-04	-0.24297087E-02	C.
70	0.94636024E-04	-0.24297097E-02	C.10780000E-04
71	0.10779747E-03	-0.23313008E-02	C.
72	0.10779737E-03	-0.23313008E-02	C.10780000E-04
73	0.47304071E-04	-0.22724085E-02	C.
74	0.47304076E-04	-0.22724081E-02	C.10780000E-04
75	-0.39802864E-04	-0.22693110E-02	C.
76	-0.39802864E-04	-0.22693116E-02	C.10780000E-04
77	-0.12036251E-03	-0.22966544E-02	C.
78	-0.12036251E-03	-0.22966543E-02	C.10780000E-04
79	-0.	-0.23238816E-02	C.
80	0.	-0.23238815E-02	C.10780000E-04
81	0.11676125E-03	-0.23108181E-02	C.
82	0.11676137E-03	-0.23108214E-02	C.10780000E-04
83	0.15176097E-03	-0.22854976E-02	C.
84	0.15176078E-03	-0.22854986E-02	C.10780000E-04
85	0.78529356E-04	-0.22755395E-02	C.
86	0.78529472E-04	-0.22755396E-02	C.10780000E-04
87	-0.11011289E-04	-0.22810224E-02	C.
88	-0.11011085E-04	-0.22810229E-02	C.10780000E-04
89	-0.12079116E-03	-0.23048334E-02	C.
90	-0.12079117E-03	-0.23048336E-02	C.10780000E-04
91	-0.	-0.22355898E-02	C.
92	0.	-0.22355897E-02	C.10780000E-04
93	0.12555477E-03	-0.22408129E-02	C.
94	0.12555478E-03	-0.22408159E-02	C.10780000E-04
95	0.15641811E-03	-0.22572506E-02	C.
96	0.15641802E-03	-0.22572512E-02	C.10780000E-04
97	0.94325136E-04	-0.22786600E-02	C.
98	0.94325036E-04	-0.22786592E-02	C.10780000E-04
99	-0.60475004E-05	-0.22951782E-02	C.
100	-0.60478437E-05	-0.22951785E-02	C.10780000E-04
101	-0.12153132E-03	-0.23265890E-02	C.
102	-0.12153135E-03	-0.23265895E-02	C.10780000E-04

Cold Transient Overshoot - Condition (d) - Sixth Calculation Loop.

YIELD CHECK AFTER 5 ITTERATIONS

ELEMENT	TOTAL STRAIN	PLASTIC STRAIN	EFFECTIVE STRESS	YIELD STRESS	SECANT MODULUS	SECANT POISSON
1	C.000522	C.	15664.2	55000.0	30000000.0	0.3100
2	0.000486	C.	14570.2	55000.0	30000000.0	0.3100
3	C.000494	C.	14820.1	55000.0	30000000.0	0.3100
4	C.000523	0.	15677.8	55000.0	30000000.0	0.3100
5	0.000506	0.	15184.3	55000.0	30000000.0	0.3100
6	C.000518	0.	15545.1	55000.0	30000000.0	0.3100
7	C.003723	0.002657	17706.7	11000.0	4755537.6	0.4513
8	0.003750	0.002680	17765.7	11000.0	4737130.1	0.4515
9	0.004614	0.003430	19659.0	11000.0	4260397.8	0.4564
10	C.004785	0.003579	20033.8	11000.0	4186433.8	0.4571
11	0.CC6317	0.004908	23388.8	11000.0	3702786.0	0.4621
12	0.006373	0.004957	23512.5	11000.0	3689401.2	0.4622
13	0.008126	0.006478	27353.9	11000.0	3366179.4	0.4655
14	0.007423	0.005868	25814.2	11000.0	3477396.1	0.4644
15	C.023940	C.022149	29736.6	17700.0	1242132.0	0.4873
16	C.023407	0.021633	29456.3	17700.0	1258424.3	0.4871
17	C.021241	C.019535	28316.4	17700.0	1333097.6	0.4863
18	C.014421	0.012932	24727.6	17700.0	1714678.5	0.4824
19	0.010756	0.009421	22820.0	17700.0	2113732.2	0.4784
20	C.022950	C.021190	29215.6	17700.0	1273018.1	0.4870
21	0.021508	0.019794	28456.8	17700.0	1323088.8	0.4865
22	C.018802	0.017174	27032.9	17700.0	1437767.4	0.4853
23	0.017781	0.016185	26455.6	17700.0	1490113.0	0.4847
24	0.015156	C.013645	25115.5	17700.0	1656887.3	0.4830
25	0.021995	C.020266	28713.?	17700.0	1305428.9	0.4866
26	C.021091	0.019390	28237.3	17700.0	1338842.9	0.4863
27	C.020352	0.018675	27848.7	17700.0	1368331.1	0.4860
28	C.019886	0.018223	27603.2	17700.0	1388086.0	0.4858
29	C.019244	C.017601	27265.3	17700.0	1416846.7	0.4855
30	0.021988	C.020259	28709.6	17700.0	1305674.6	0.4866
31	C.021006	0.019308	28192.8	17700.0	1342115.5	0.4863
32	C.021258	0.019552	28325.4	17700.0	1332447.3	0.4864
33	0.022557	0.020810	29009.0	17700.0	1286017.1	0.4868
34	C.022866	0.021109	29171.7	17700.0	1275743.2	0.4869

REFERENCES

1. Miller, R.W., RETSCP: A Computer Program for Analysis of Rocket Engine Thermal Strains with Cyclic Plasticity, NASA CR-134640, June 1974.

2. Langer, B.F., Fatigue Failure from Stress Cycles of Varying Amplitude, Journal of Applied Mechanics, 1937.

3. Zienkiewicz, O.D., The Finite Element Method in Engineering Science, McGraw Hill Publishing Company, Ltd., 1971.

4. Wang, C., Applied Elasticity, McGraw Hill Book Company, New York, 1953.

5. Smith, R.W., Hirschberg, M.H., and Manson, S.S., Fatigue Behavior of Materials Under Strain Cycling in Low and Intermediate Life Range, NASA TN D-1574, 1963.

6. Mendelson, A., Plasticity: Theory and Application, The MacMillan Company, 1968.

7. Jackson, C.R., Hall, A.M., and Schwope, A.D., Comparative Properties of Several Types of Commercial Coppers, as Cold-Worked and as Recrystallized, AIME Tech., Pub. 2274, 1947. Data from above available through Copper Data Center, Copper Development Association, Battelle Columbus Laboratories.

8. Schwartzbart, H., and Brown, W.F., Notch-Bar Tensile Properties of Various Materials and Their Relation to the Unnotch Flow Curve and Notch Sharpness, Transactions of the ASM, Vol. 46, 1954.

REFERENCES, Cont'd.

9. Manson, S.S., Thermal Stress and Low-Cycle Fatigue, McGraw Hill Book Company, 1966.

10. Conway, J.B., Stente, R.H., and Berling, J.T., High Temperature, Low-Cycle Fatigue of Copper-Base Alloys in Argon, Part I - Preliminary Results for 12 Alloys at 1000°F (538°C), NASA CR-121259, January, 1973.

11. Upthegrove, C., and Burghoff, H.L., Elevated - Temperature Properties of Coppers and Copper-Base Alloys, ASTM No. 181, 1956.

12. Coffin, C.F., and Tavernelli, J.F., The Cyclic Straining and Fatigue of Metals, Transactions of the Metallurgical Society of AIME, Vol. 215, October, 1959.

13. Wood, W.A., and Segal, R.L., Softening of Cold-Worked Metal by Alternating Strain, Journal of the Institute of Metals, Vol. 86, 1958.

14. Manson, S.S., The Challenge to Unify Treatment of High Temperature Fatigue, A Partisan Proposal Based on Strainrange Partitioning, ASTM STP-520, 1973.

15. Manson, S.S., Fatigue, A Complex Subject - Some Simple Approximations, Experimental Mechanics, July, 1965.

16. Manson, S.S., and Halford, G., A Method of Estimating High Temperature Low Cycle Fatigue Behavior of Materials, NASA TM-X-52270, 1967.

REFERENCES, Cont'd.

17. Conway, J.B., Stentz, R.H., and Berling, J.T., High Temperature, Low-Cycle Fatigue of Copper Base Alloys in Argon; Part III - Zirconium - Copper; Thermal - Mechanical Strain Cycling, Hold-Time and Notch Fatigue Results, NASA CR-121261, December, 1973.

18. Sorensen, A., A General Theory of Fatigue Damage Accumulation, Journal of Basic Engineering, March, 1969.

19. Shoji, J.M., Advanced Hydrogen/Oxygen Thrust Chamber Design Analysis, NASA CR-121213, December, 1973.